A framework to quantify phenotypic and genotypic parallel evolution

Maddie E. James[1*], Melanie J. Wilkinson[1], Henry L. North[1,2], Jan Engelstädter[1], Daniel Ortiz-Barrientos[1]

[1]The University of Queensland, School of Biological Sciences, St. Lucia QLD 4072, Australia. [2]Current address: University of Cambridge, Department of Zoology, Downing St., Cambridge CB2 14 3EJ, UK

Short title: Parallel evolution in *Senecio*

* Corresponding author

Email: maddie.james@uqconnect.edu.au (MEJ)

Abstract

The independent and repeated adaptation of populations to similar environments often results in the evolution of similar forms. This phenomenon creates a strong correlation between phenotype and environment and is referred to as parallel evolution. However, there is ongoing debate as to when we should call a system either phenotypically or genotypically 'parallel.' Here, we suggest a novel and simple framework to quantify parallel evolution at the genotypic and phenotypic levels. Our framework combines both traditional and new approaches to measure parallel evolution, and categorizes them into broad- and narrow-sense scales. We then apply this framework to coastal ecotypes of an Australian wildflower, *Senecio lautus*, that have evolved in parallel. Our findings show that *S. lautus* populations inhabiting similar environments have evolved strikingly similar phenotypes. These phenotypes have arisen via mutational changes occurring in different genes, although many share the same biological functions. Our work paves the way towards a common framework to study the repeated evolution of forms in nature.

Author summary

When organisms face similar ecological conditions, they often evolve similar phenotypic solutions. When this occurs in closely related taxa, it is referred to as parallel evolution. Systems of parallel evolution provide some of the most compelling evidence for the role of natural selection in evolution, as they can be used as natural replicates of the adaptation process. However, there is debate as to when we should call a system 'parallel'. This debate stems back to the mid 1900s, and although there have been multiple attempts within the literature to clarify terminology, controversy still remains. In this study, we propose a novel framework to quantify phenotypic and genotypic parallel evolution within empirical systems, partitioning parallelism into broad- and narrow-sense components. Our framework is applicable to non-model organisms and provides a common set of analyses to measure parallel evolution, enabling researchers to compare the extent of parallel evolution across different study systems. In turn, this helps to reduce confusion surrounding the term 'parallel evolution' at both the phenotypic and genotypic levels. We then apply our framework to two coastal ecotypes of an Australian plant, *Senecio lautus*. We show that similar phenotypes within each ecotype have evolved via mutational changes in different genes, though some are involved in similar biological functions. Our research not only helps to consolidate the field of parallel evolution, but paves the way to understanding the role of natural selection in the repeated evolution of similar phenotypes within nature.

Introduction

When populations independently and repeatedly adapt to similar environments, they often evolve similar phenotypes (Schluter, 2000). This has been observed in a wide variety of animal taxa (e.g., Johannesson *et al.*, 1993; Nosil *et al.*, 2002; Elmer *et al.*, 2010; Ravinet *et al.*, 2013; Soria-Carrasco *et al.*, 2014; Perreault-Payette *et al.*, 2017) and in some plants (e.g., Foster *et al.*, 2007; Trucchi *et al.*, 2017; Cai *et al.*, 2019; Konečná *et al.*, 2019). When independent populations evolve from similar initial conditions, this phenomenon is referred to as 'parallel evolution' (Schluter & Nagel, 1995; Bolnick *et al.*, 2018). The correlation that arises between phenotype and environment during parallel evolution provides strong evidence for the role of natural selection in creating new forms. This is because it is unlikely that similar phenotypes would have evolved multiple times purely by chance (Lenormand *et al.*, 2009, but see Losos, 2011). Systems of parallel evolution are unique as they provide natural replicates of the evolutionary process, enabling researchers to study the genetics and ecology of how adaptation proceeds in nature (Lenormand *et al.*, 2016). Such systems can also shed light on the level at which evolution is repeatable and predictable (Stern & Orgogozo, 2009; Blount *et al.*, 2018).

The evolution of similar phenotypes within the same environment can arise via independent and repeated selection on the same nucleotide site or gene (reviewed in Wood *et al.*, 2005; Christin *et al.*, 2010; Stern, 2013). Similar phenotypes can also arise by selection on entirely different genes, although often from the same functional pathway (e.g., Smith & Rausher, 2011; Kowalko *et al.*, 2013; Roda *et al.*, 2013b; Laporte *et al.*, 2015; Perreault-Payette *et al.*, 2017; Cassin-Sackett *et al.*, 2019). Here, different genetic routes are able to produce similar phenotypic outcomes across populations, even though selection does not act upon the same allele or gene. Within the literature there is controversy as to which level of biological organization (nucleotide site, gene, or biological function) should be viewed as genotypically 'parallel'. This makes it difficult to conceptualize both phenotypic and genotypic parallel evolution.

The debate surrounding the term parallel evolution remains sprightly but confusing (Haas & Simpson, 1946; Arendt & Reznick, 2008; Lenormand *et al.*, 2016; Stuart, 2019; Thompson *et al.*, 2019). Some researchers argue that *parallel* systems arise only when the same nucleotide site or gene is repeatedly involved in the evolution of similar phenotypes (Rosenblum *et al.*, 2014). However, others maintain that when similar phenotypes independently arise, they

should be classed as cases of parallel evolution regardless of the underlying genetics (e.g., Lim *et al.*, 2019). Some argue that the term *parallel* should be disregarded altogether and replaced with *convergence* (Arendt & Reznick, 2008). Although there are also several incompatible definitions of *convergent evolution* and *parallel evolution* (Stern, 2013), it is generally accepted that *convergence* refers to the evolution of similar forms from distantly related taxa, whereas *parallel* is the evolution of similar forms from similar initial conditions in closely related taxa – terminology that we are also adopting here (Speed & Arbuckle, 2017; Bolnick *et al.*, 2018 but see Stern, 2013; Lenormand *et al.*, 2016). To reduce the ensuing confusion when the term *parallel evolution* is used in isolation, some researchers have proposed we should separate *parallel evolution*, or *parallelism*, into two distinct components: the phenotype and the genotype (Elmer & Meyer, 2011).

Even though separating *parallel evolution* into phenotypic and genotypic components helps reduce confusion, researches often implement different statistical approaches to measure parallelism across different study systems. These different approaches can lead to different interpretations of parallel evolution at the level of the phenotype and genotype (Bolnick *et al.*, 2018), which in turn makes it difficult to directly compare between studies. It becomes evident we require common approaches to measure parallelism so researchers can not only quantify the extent of parallel evolution within a given system, but also compare the amount of parallelism between systems.

A framework to measure parallel evolution

We propose a novel and simple framework to measure phenotypic and genotypic parallel evolution (Figure 1). Our framework synthesizes traditional and new approaches, and partitions these measures of parallelism into the broad- and narrow-sense scales. This partitioning allows researchers to gain information not only about the overall patterns within a system but also the specific similarities of replicate populations. We show that different measures of parallelism can reveal how natural selection creates patterns at different scales of phenotypic and genotypic variation.

To characterize the extent of phenotypic and genotypic parallelism within a system, it is necessary to rigorously demonstrate that populations adapting to similar environments (collectively referred to as an ecotype) have arisen multiple times independently. We refer the reader to our previous analyses of parallel evolution in *Senecio lautus* (Roda *et al.*, 2013b;

James *et al.*, 2020) and to systems such as the marine snail, *Littorina saxatilis* (Quesada *et al.*, 2007; Johannesson *et al.*, 2010; Bierne *et al.*, 2013; Butlin *et al.*, 2014; Pérez-Pereira *et al.*, 2017), and the threespine stickleback, *Gasterosteus aculeatus* (Colosimo *et al.*, 2005; Chan *et al.*, 2010; Dean *et al.*, 2019; Marques *et al.*, 2019) where one can find some of the strongest evidence for the independent origin of populations, and to the increasing number of potential cases of parallel evolution in plants (Foster *et al.*, 2007; Ostevik *et al.*, 2012; Trucchi *et al.*, 2017; Cai *et al.*, 2019; Konečná *et al.*, 2019; Knotek *et al.*, 2020).

Phenotypic parallel evolution. Researchers of parallelism traditionally ask to what extent ecotypes are phenotypically distinct and which traits contribute to these differences (see Bolnick *et al.*, 2018 for a detailed review of approaches). More recently, studies of parallelism (e.g., Elmer *et al.*, 2014; Kusche *et al.*, 2015; Oke *et al.*, 2017; Stuart *et al.*, 2017; Paccard *et al.*, 2019; Pilakouta *et al.*, 2019; Jacobs *et al.*, 2020) have shifted to also quantify phenotypic similarities between each replicate population pair using geometric approaches such as phenotypic change vector analysis (Collyer & Adams, 2007; Adams & Collyer, 2009; Collyer *et al.*, 2015). Unfortunately, geometric approaches do not quantify overall differences between ecotypes, so replicate pairs can show little parallelism yet contribute to strong parallel phenotypic differences between ecotypes. To maximize the benefits of both methods we propose to quantify phenotypic and genotypic parallelism with multiple approaches, which can be classified at broad- and narrow-sense scales (Figure 1).

In the broad-sense, phenotypic parallelism quantifies the net contribution of all replicate populations within each ecotype to the overall phenotypic differences between ecotypes (Figure 1). It can be broken into two components: ‘parallel ecotype’, and ‘parallel trait’. ‘Parallel ecotype’ describes the multivariate differences between ecotypes, such that a highly parallel system would show no overlap in the trait space occupied by each ecotype. ‘Parallel trait’ describes which univariate traits are different between ecotypes such that they can easily predict the habitat in which an individual lives, from trait attributes alone. In the narrow-sense, phenotypic parallelism quantifies and compares similarities between each replicate population pair (which we have called ‘parallel pair’). Narrow-sense parallelism gives insight into which pairs are most similar to each other, and which pairs deviate from the common trend within the system (Figure 1). These levels of phenotypic parallelism reveal both the net contribution of replicate pairs to the general differences between ecotypes

(broad-sense), as well as the relative similarities in divergence between each replicate population (narrow-sense).

Genotypic parallel evolution. Researchers of genotypic parallelism often measure the proportion of shared outlier loci between replicate populations to ask whether the same alleles or genes are responsible for the evolution of similar phenotypes (Wood *et al.*, 2005). In most cases, this will be difficult because causal alleles might not be sampled (Catchen *et al.*, 2017; Lowry *et al.*, 2017; McKinney *et al.*, 2017), only their indirect linkage effects might be detected by outlier loci (Hoban *et al.*, 2016), and random fixations can accumulate between populations over time as genetic drift increases dissimilarity between population pairs. If knowledge of causal alleles is available, then one must demonstrate that a given site has been under repeated and independent selection in each replicate pair (Lee & Coop, 2017, 2019). Typically, these analyses are undertaken comparing individual replicate pairs (e.g., Roda *et al.*, 2013b; Lamichhaney *et al.*, 2017; Cassin-Sackett *et al.*, 2019), although some studies detect broad, or 'global' outliers by comparing the aggregate of all populations within each ecotype (e.g., Jones *et al.*, 2012; Kautt *et al.*, 2012). In the absence of repeated selection on the same allele or gene, parallelism can be manifested at the functional level, such that different genes under selection participating in the same predicted biological function contribute to the pattern of phenotypic parallelism in a system. It is frequently asked whether predicted biological functions are consistently enriched across independent populations (Smith & Rausher, 2011; Kowalko *et al.*, 2013; Roda *et al.*, 2013b; Perreault-Payette *et al.*, 2017; Cassin-Sackett *et al.*, 2019). These analyses can inform us about how genotypically parallel a system is at different scales of divergence, so we can also view genotypic parallel evolution as broad-sense or narrow-sense (Figure 1).

Broad-sense genotypic parallelism quantifies the net contribution of all replicate populations within each ecotype to the overall genetic differences between ecotypes (Figure 1). We can measure it at different levels of biological organization: the nucleotide site, gene, and biological function. For instance, a highly parallel nucleotide site would clearly differentiate the two ecotypes. Such parallel alleles might have originated repeatedly and independently gone to fixation in each population inhabiting similar habitats, or might have recurrently increased in frequency from standing genetic variation. Broad-sense parallelism at the level of the biological function asks which, if any, predicted functions are enriched with divergent

genes between the ecotypes. An enriched function might suggest it has been repeatedly involved in adaptation across replicate populations.

On the other hand, narrow-sense genotypic parallelism quantifies which outlier nucleotide sites and genes are the most similar across replicate pairs, and how similar the enriched biological functions are for each pair (Figure 1). It asks which genetic differences distinguish the ecotypes of each replicate pair and at what level of organization. Patterns of genotypic divergence can be complex and create a mismatch between genotypic and phenotypic parallelism. For instance, all replicate pairs might have biological functions that diverged in parallel, but in each case recruiting different genes. This will lead to lack of genotypic parallelism at the nucleotide site and gene level both in the broad- and narrow-sense. Such a system can still be highly parallel at the phenotypic level. We expect this to be common when parallel evolution occurs on complex traits via polygenic adaptation (Gompel & Prud'homme, 2009; Ralph & Coop, 2010; Rosenblum *et al.*, 2014; Yeaman, 2015; MacPherson & Nuismer, 2017).

Overall, our framework is particularly useful for systems with the repeated and independent origin of populations, where pairs of ecotypes have adapted to contrasting environments. Nevertheless, our framework can also be used for single origin systems containing multiple secondary contacts with gene flow between ecotypes, or species. In this case, researchers can still examine the dynamics of repeated population divergence and parallel maintenance of species differences in the face of gene flow, but cannot interpret populations as being from independent origins. Here, we examine the extent of phenotypic and genotypic parallel evolution within an Australian wildflower species complex, *Senecio lautus*. We use both broad- and narrow-sense measures and demonstrate the importance of quantifying parallelism at these different scales of divergence.

The *Senecio lautus* species complex

The *Senecio lautus* species complex contains a variety of ecotypes adapted to contrasting environments. The Dune and Headland ecotypes are of particular interest as they consist of multiple parapatric Dune-Headland population pairs along the Australian coastline that are often sister groups in the phylogeny (Roda *et al.*, 2013a; Melo *et al.*, 2019; James *et al.*, 2020). Despite the close geographic proximity between populations of a pair (i.e., ecotypes within each locality), there is little to no gene flow between them, suggesting a large number

of independent and repeated origins (James *et al.*, 2020). There is a strong association between overall morphology and habitat in this coastal system: Dune plants, colonizing the sandy dunes, are erect with few branches, whereas Headland individuals grow on rocky headlands and are prostrate with many branches (Figure 2D). Populations maintain their phenotypes when grown in common garden conditions (Walter *et al.*, 2016, 2018a; Wilkinson *et al.*, 2020), suggesting that phenotypic plasticity within the system is weak. Previous work with *S. lautus* in common garden conditions has identified a suite of divergent traits between Dune and Headland populations, which include characteristics related to plant architecture and leaf morphology (Walter *et al.*, 2018a). However, we lack a comprehensive characterization of how parallel the phenotypes and genotypes are within natural populations, and how this affects divergence at the level of the ecotype and replicate population pair.

To assess the extent of phenotypic and genotypic parallelism in *S. lautus*, we used 22 populations: nine replicate Dune-Headland pairs, two allopatric Dune populations, and two allopatric Headland populations. We first quantify how phenotypically distinct the Dune and Headland ecotypes are, and which replicate pairs are the most phenotypically similar. We then build on previous work (Roda *et al.*, 2013b) to ask whether similar genetic mechanisms underlie these repeated phenotypes (i.e., repeated selection on the same nucleotide site, gene, or biological function). In addition, we ask whether the variation in the extent of parallelism can be attributed to non-stochastic factors, including levels of gene flow and within ecotypic environmental variation.

Methods

Phenotypic parallelism

Sample collection. To quantify the extent of phenotypic parallelism within *S. lautus*, we measured a suite of plant architecture and leaf morphology traits from 20 Dune and Headland populations along the coast of Australia (n_{mean} = 30 individuals, n_{total} = 605; Figures 2A, 2B; Table S1). These populations include eight Dune-Headland pairs along a continuum from geographically parapatric to allopatric (four of which are sister taxa), as well as four allopatric populations that do not have a parapatric pair (as inferred from previous phylogenetic analyses; James *et al.*, 2020). We sampled mature (flowering) plants evenly across the geographic range of each population, ensuring that each plant was more than one meter apart. We measured six plant architecture traits (vegetative height, widest width,

narrowest width, main stem angle, main stem diameter, and secondary branch angle) and eight leaf traits (area, perimeter, width, height, elongation, compactness, dissection and circularity; defined in Table S2). All plant architectural traits were measured in the field, and we sampled three secondary branch leaves per plant for leaf morphometric analysis in ImageJ v1.51 (Schneider *et al.*, 2012). Leaves were scanned at 600 dpi on a CanoScan 9000F scanner and ImageJ was used to automatically extract leaf shape characteristics. Some of the same populations and traits have been previously measured in common garden conditions (Walter *et al.*, 2018a). Overall, phenotypes in the wild are highly correlated with those measured under controlled conditions (Wilkinson *et al.*, 2020).

In ~11% of sampled plants, we were unable to measure all six plant architectural traits (such as main stem diameter and main stem angle). In these cases, we took the average of the population to impute the trait value for that individual. We ran the below analyses with and without these individuals and obtained consistent results. We report the analyses undertaken using the population means for the missing data. All phenotypic analyses were undertaken in R v3.4.2 (R Core Team, 2017). Traits were log transformed and standardized to have a mean of 0 and standard deviation of 1. We calculated pairwise correlations between all traits and removed five traits with high correlations across all populations (>0.8; Table S2). These correlated traits added minimal additional phenotypic information and are thus effectively redundant.

Relative contributions of broad- and narrow-sense phenotypic parallelism

We initially assessed the relative contributions of broad- and narrow-sense phenotypic parallelism within *S. lautus*. More specifically, we performed linear models at the multivariate level of the ecotype (MANOVA: $traits = ecotype + pair + ecotype \times pair$), as well as the univariate level of each trait (ANOVA: $trait = ecotype + pair + ecotype \times pair$) and extracted the partial effect sizes (partial η^2; Langerhans & DeWitt, 2004) for each term in the ANOVAs, (and Wilk's partial η^2 for the MANOVA) using the *etasq* function in the *heplots* package (Fox *et al.*, 2018) in R. As these models require population pairs, we excluded two Headland allopatric populations (H03 and H07) and two Dune allopatric populations (D09 and D35). The partial effect size of the *ecotype* term denotes how much of the phenotypic variation is explained by the overall differences between ecotypes, whereas the *pair* and *interaction* terms indicate how much variation is unique to replicate pairs. Therefore, when the effect size for the *ecotype* term is larger than the *pair* or *interaction*, this

indicates that broad-sense phenotypic parallelism might predominate over narrow-sense, although there still might be a strong influence of differences between replicate pairs. After assessing these relative contributions (at the level of the ecotype and trait), we further explored the detailed patterns of broad- and narrow-sense phenotypic parallelism within *S. lautus*.

Broad-sense phenotypic parallelism

Parallel ecotype. To ask whether ecotypes are phenotypically distinct within multivariate space, we performed a one-way MANOVA (MANOVA: *traits* = *ecotype*) across the 20 Dune and Headland populations, where *traits* denotes the multivariate response variable of all traits, and *ecotype* is a fixed effect of Dune or Headland. We also split traits into a plant architectural and a leaf trait-set to ask whether phenotypic differences between ecotypes depend on the trait category. To ask whether we can predict the ecotype each individual belongs to, based on their phenotype, we performed K-means clustering with the Hartigan-Wong algorithm (Hartigan & Wong, 1979). We used 25 random initial configurations and retained the run with the smallest sums of squares of the individuals to their assigned cluster center, and then calculated the proportion of individuals assigned to their correct ecotype. We also performed a linear discriminant analysis across all traits to ask which linear trait combination best explains the phenotypic differences between Dune and Headland ecotypes.

Parallel trait. To ask which univariate traits are the most parallel between the Dune and Headland ecotypes we undertook three approaches: vote-counting, trait-by-trait linear models, and R^2 analysis. As the vote-counting and linear model approaches require population pairs, we again excluded the four allopatric populations (H03, H07, D09 and D35). For vote-counting, we calculated the mean trait value for the Dune and Headland of each replicate pair and asked whether there was a consistent increase or decrease in the trait value for all replicate pairs (two-sided dependent-samples sign-tests). However, this vote-counting approach ignores trait effect-size, and also has low statistical power when the sample size (number of replicate pairs) is small. Therefore, we also used trait-by-trait linear models (*trait* = *ecotype* + *pair* + *ecotype* × *pair*) to ask whether there was a significant main effect of ecotype for each trait. To also quantify the extent of phenotypic parallelism between ecotypes, we extracted the proportion of phenotypic variance explained by the ecotype term (R^2) for each trait from one-way ANOVAs performed on the population means (see Langerhans, 2018). Following Langerhans (2018), we considered a trait strongly parallel

296 when $R^2 \geq 0.50$, moderately parallel when $0.50 > R^2 \geq 0.33$, and weakly parallel when $R^2 <$
297 0.33. We then examined which traits were consistently viewed as parallel across each of the
298 three approaches.

299 **Narrow-sense phenotypic parallelism**

300 **Parallel pair.** To quantify the specific phenotypic similarities and differences between
301 replicate population pairs, we used Phenotypic Change Vector Analysis (PCVA; Collyer &
302 Adams, 2007; Adams & Collyer, 2009; Collyer *et al.*, 2015). Within multivariate phenotypic
303 space, PCVA quantifies both 1) the amount of divergence, and 2) the contribution of traits to
304 divergence between replicate pairs. The procedure is as follows: the phenotypic centroid
305 (multivariate mean) is calculated per population. For each population pair, their centroids are
306 connected with a vector. The length (L) of this vector quantifies how divergent the two
307 populations are – the longer the length, the more divergent. The difference in length (ΔL)
308 between vectors thus denotes the difference in the magnitude of divergence between two
309 replicate population pairs. The two pairs are considered parallel with regards to the
310 magnitude of their divergence if ΔL is not statistically different from zero ($\Delta L \approx 0$; Bolnick *et*
311 *al.*, 2018).

312 The contribution of traits to divergence is measured by the angle between vectors (θ). A large
313 angle between two pairs ($\theta >> 0°$) suggests the traits contributing to population divergence
314 are quite different between the pairs. The contribution of traits is considered parallel when the
315 angle is not statistically different from zero ($\theta \approx 0°$). Using R code modified from Collyer &
316 Adams (2007), we calculated ΔL and θ for all pairwise comparisons between replicate pairs
317 and performed permutations to test for statistical significance (see *Supplementary R code* for
318 details). To ensure this analysis was robust and not dominated by a single trait, we repeated
319 the calculations of ΔL and θ nine times with removing a single trait each time. We observed
320 consistent results across all calculations, suggesting our results are not dominated by a single
321 trait (results not shown).

322 **Genotypic parallelism**

323 **Sequencing and bioinformatics.** To quantify the extent of genotypic parallelism within *S.*
324 *lautus*, we collected leaf samples from nine population pairs along the coast of Australia
325 ($n_{mean} = 56$, $n_{total} = 1009$; Figures 2A, 2B; Table S1). DNA was extracted using a modified

CTAB protocol (Clarke, 2009). We created reduced representation (RAD) libraries by using a two-enzyme Genotyping-by-Sequencing (GBS) approach (modified from Poland *et al.*, 2012), with Pst1 and Msp1. We created seven equimolar pools (192 individuals per pool), which were size-selected on the BluePippin (2% DF Marker V1, 300-500bp; Sage Science). Pooled libraries were sent to Beijing Genomics Institute (BGI) for sequencing on seven lanes of the HiSeq4000, with 100bp paired-end sequencing.

BGI removed forward barcodes and quality filtered the raw reads to remove reads containing Illumina adaptors, low quality reads (> 50% of bases < Q10), and reads with > 10% Ns. We trimmed reverse barcodes with *TagCleaner* standalone v0.12 (Schmieder *et al.*, 2010). Reads were mapped to the *S. lautus* reference PacBio genome v1.0 (Wilkinson *et al.*, 2020) with *BWA-MEM* v0.7.15 (Li & Durbin, 2009; Li, 2013). *PicardTools* v2.7.0 (Broad Institute, 2019) was used to clean aligned reads and to add read groups (PCR duplicates were not marked for removal). We jointly called all variant and invariant sites for each population with *FreeBayes* v1.1.0 (Garrison & Marth, 2012). Using *VCFtools* v0.1.15 (Danecek *et al.*, 2011), we retained sites if they were present in > 50% of individuals, had a minimum quality score of 30, and a minimum minor allele count of 1. We then filtered for a minimum depth of 3 for a genotype call. Individuals were removed if they contained > 40% missing data. We then filtered for a maximum mean depth of 100, and a minimum mean depth of 10. We filtered for missing data per population, removing sites if they contained > 50% of missing data within each population. We refiltered for an overall missing data of 20%. Indels were removed with *vcflib* (Garrison, 2016). We then filtered for population-specific Hardy Weinberg Equilibrium using the *filter_hwe_by_pop.pl* script within *dDocent* (Puritz *et al.*, 2014). We filtered for an overall minor allele count of 5, retaining 9,686 variable sites across all populations. See James *et al.*, (2020) for further details on DNA extraction, library preparation and bioinformatics.

Broad-sense genotypic parallelism

Parallel nucleotide site. We first assessed the relative contributions of broad- and narrow-sense parallelism for each of the 9,686 sequenced SNPs across populations. More specifically, we first used PLINK v1.9 (Purcell *et al.*, 2007) to normalize each SNP by conducting a PCA and extracting the first eigenvector. For each SNP we then performed linear models (ANOVA: $SNP = ecotype + pair + ecotype \times pair$) and we extracted the partial effect sizes (partial η^2) for each term in the model. As above, the partial effect size of

the *ecotype* term denotes how much of the variation for each SNP is explained by the overall differences between ecotypes, whereas the *pair* and *interaction* terms indicate how much variation is unique to replicate pairs. Therefore, when the effect size for the *ecotype* term is larger than the *pair* or *interaction*, this indicates that broad-sense predominates over narrow-sense. To plot these data as a frequency distribution, we calculated each SNP's distance from a 1:1 line by subtracting the effect size for either the *pair* or *interaction* term from the *ecotype* term in the model. Positive values indicate a larger contribution of broad- over narrow-sense parallelism, and vice versa for negative values.

After assessing these relative contributions, we further explored the detailed patterns of broad-sense parallelism at the level of the nucleotide site. To this end, we combined a number of approaches to detect outliers between the Dune and Headland ecotypes. To ask which nucleotide sites distinguish the ecotypes (overall Dune vs Headland), we undertook two approaches: 1) detection of outliers comparing all Dune populations vs all Headland populations, and 2) detection of outliers separately for each Dune-Headland pair, and then asked whether there were concordant allele frequency differences across all pairs.

Approach 1: To detect broad-sense outliers between the ecotypes, we undertook three outlier detection methods: the top 1% from the distribution of F_{ST} values, the top 1% from the distribution of cluster separation scores (CSS), and those SNPs identified by *BayeScan* (Foll & Gaggiotti, 2008). To remove low frequency variants (Bhatia *et al.*, 2013), we filtered this dataset for MAF 0.05, retaining 9,269 SNPs. F_{ST} per SNP (Weir & Cockerham, 1984) was calculated within *VCFtools* (Danecek *et al.*, 2011), and we selected the top 1% (corresponding to $F_{ST} > 0.353$, which also corresponds to an average change in allele frequency, Δp, of 0.47, SD = 0.080; Figure S1A). We calculated the cluster separation score (CSS; Jones *et al.*, 2012) per SNP using a custom R script (see *Supplementary R code* for details). CSS is a genetic distance-based measure that quantifies the average divergence between Dune and Headland clusters, after accounting for the variance within each ecotype. It ranges between 0 and 1, with higher values indicating a more distinct separation between Dune and Headland ecotypes. We selected the top 1% of CSS (corresponding to CSS > 0.523, an average Δp of 0.45, SD = 0.087; Figure S1B). We also detected outliers in *BayeScan* v2.1 (Foll & Gaggiotti, 2008). *BayeScan* implements a reversible-jump MCMC algorithm to estimate posterior odds comparing a model with and without selection for each SNP. We used default parameters with a prior odd of ten, meaning the neutral model is ten

times more likely than the model with selection (as recommended for datasets of our size; Foll & Gaggiotti, 2008). Results were robust to increasing the prior odds to 100 (data not shown). We categorized SNPs as highly differentiated if they contained a posterior probability > 0.91, corresponding to a Bayes Factor of > 10, and corresponding to an average Δp of 0.38, SD = 0.121. For approach 1, we classified SNPs as outliers if they were detected in at least two of the three methods (Figure S1C).

Approach 2: To detect more subtle signals of broad-sense outliers between the ecotypes, we asked whether there were concordant allele frequency changes across replicate pairs. Specifically, we first detected outliers separately for each Dune-Headland pair (see methods below). If a nucleotide site was highly differentiated in at least one pair, we compared allele frequencies across all pairs for the site, and we asked whether the Δp for each replicate pair was in the same direction across all pairs (tested using two-sided dependent-samples sign-tests in R). Our overall best candidates for broad-sense SNP parallelism are those that overlap between the two methods, i.e., they show high differentiation between ecotypes (approach 1), with concordant allele frequency changes across replicate pairs (approach 2).

To ask whether the candidate outliers from any of the approaches above fall within genic or non-genic regions, we mapped a previously created *S. lautus* transcriptome (Liu, 2014) to the reference PacBio genome v1.0 (Wilkinson *et al.*, 2020) with *minimap2* v2.17 (Li, 2018) using default parameters. We considered each transcript a separate gene, which included all isoforms. As the transcriptome excludes introns, we still considered SNPs mapped to the reference genome that fall between two segments of the same transcript as a genic SNP. All other SNPs were considered non-genic, which are expected to include variants in regulatory and repetitive regions as well as in genic regions with unknown homologous genes in other plants. We excluded SNPs that had > 1 gene mapping to it.

Parallel gene. We assessed the relative contributions of broad- and narrow-sense parallelism for each gene across populations. We again normalized the data, retaining the first eigenvector for each gene. For each gene we then performed linear models (ANOVA: *gene* = *ecotype* + *pair* + *ecotype* × *pair*) and we extracted the partial effect sizes (partial η^2) for each term in the model. We again plotted this as a frequency distribution (see above for details). After assessing these relative contributions, we further explored the detailed patterns of broad parallelism at the level of the gene according to the outlier analysis above. More specifically, we considered a gene an outlier if it harbored at least one outlier SNP according to the two

above approaches (i.e., showed high differentiation between ecotypes (approach 1), with concordant allele frequency changes across replicate pairs (approach 2)). We asked whether the broad-sense nucleotide-site outliers were located across multiple genes or the same gene. To assign orthologous genes, we used *BLASTx* (Altschul *et al.*, 1990) to obtain a RefSeq code (Pruitt, 2004) for each *S. lautus* gene. We searched the RefSeq protein database for *Arabidopsis thaliana* proteins that match our target genes using an E-value threshold of $< 10^{-6}$. We used the web-based version of *DAVID* v6.8 (Huang *et al.*, 2009b; a) to obtain the predicted functional annotation of each *S. lautus* gene sequenced in this work.

Enriched biological function. To ask whether the outliers were enriched for any functional categories, we used *DAVID* to conduct a gene-enrichment analysis using functional annotation clustering. Functional annotation clustering groups similar functional terms into clusters to avoid redundant annotations. We considered a cluster as enriched if at least one category within the cluster had a P-value < 0.05. This P-value is the EASE score, a modified Fisher Exact P-value. In addition, we applied more stringent criteria for selecting enriched clusters (Benjimani-adjusted P < 0.05 and False Discovery Rate < 1). The *Arabidopsis thaliana* genome was used as a genetic background.

Narrow-sense genotypic parallelism

Parallel nucleotide site. We asked which nucleotides sites are highly differentiated (i.e., outliers) in each replicate pair, and whether the same nucleotide sites are outliers across multiple pairs (i.e., across multiple localities). We first filtered each separate pair for MAF 0.05, retaining between 5,513 and 8,875 SNPs per pair (mean = 7,461 SNPs; SD = 1,038). As above, we identified outliers for each replicate pair using a combination of F_{ST}, CSS, and *BayeScan*. Instead of selecting the top 1% of F_{ST} and CSS values (which is highly dependent on the number of sampled SNPs) we chose stringent cut-offs of F_{ST} and CSS > 0.95. Within *BayeScan*, we considered SNPs with a posterior probability > 0.91 as highly differentiated, which corresponds to a Bayes Factor > 10. We considered a SNP an outlier if it was detected in at least two of the approaches. We used custom R scripts to calculate the overlap of outliers across replicate pairs. To ask whether the outliers shared between pairs were greater than expected by chance, we used a hypergeometric distribution function, *phyper*, within R to evaluate the likelihood of sharing outliers between localities.

Parallel gene. As above, we considered a gene to be an outlier if it harbored at least one differentiated SNP, and used *DAVID* to obtain the functional annotation of each gene. We again used a hypergeometric distribution to ask whether shared outlier genes between localities were greater than expected by chance.

Parallel biological function. For each replicate pair, we conducted a gene-enrichment analysis using functional annotation clustering in *DAVID* (as described above). For each pair we selected clusters containing at least one significantly enriched functional term (P-value < 0.05. This P-value is the EASE score, a modified Fisher Exact P-value). We then compared these enriched clusters across pairs to ask whether any biological functions were repeatedly enriched across pairs. We used a two-sided dependent-samples sign-test to ask if the number of enriched pairs per predicted functional category differed from chance. We compared the distributions of the proportions of shared outlier nucleotide sites, outlier genes and enriched biological functions across pairs using a two-sided X^2-test with continuity correction in R using the *prop.test* function. In addition, we applied more stringent criteria for selecting enriched clusters (Benjimani-adjusted P < 0.05 and FRD < 1), and also compared these clusters across replicate pairs.

Variation in phenotypic parallelism

We asked whether the variation in phenotypic parallelism within the system (i.e., differences in divergence (ΔL) and the contribution of traits (θ) between replicate pairs) could be explained by demographic factors. All analyses were undertaken in R. Specifically, we used gene flow estimates from James *et al.,* (2020) to ask whether gene flow constrains divergence, where we predict pairs with higher gene flow to be more phenotypically similar (linear model: *phenotypic length (L) = gene flow*; Table S3). As most pairs experience minimal gene flow and are effectively allopatric, we do not expect gene flow to be a major constraining force for most population pairs. We also used divergence time estimates from James *et al.*, (2020) to ask whether older pairs show more phenotypic divergence than younger pairs as they have experienced more genetic drift over time (linear model: *phenotypic length (L) = divergence time*; Table S3). We also reasoned that populations adapting to more contrasting environments should have greater phenotypic differences (linear model: *phenotypic length (L) = environmental distance*; Table S3). We used environmental distances from previous work in *S. lautus* (see Roda *et al.*, 2013b). In addition, we asked whether pairs that were more phenotypically similar (ΔL and θ) shared more outlier

nucleotide sites, genes, and biological functions using Mantel tests (Mantel, 1967) with 999 permutations.

Results

Relative contributions of broad- and narrow-sense phenotypic parallelism

At the multivariate level of the ecotype (MANOVA: *traits* = *ecotype* + *pair* + *ecotype* × *pair*), the partial effect size of the ecotype term (Wilks partial $\eta^2 = 0.86$) was larger than both the pair (Wilks partial $\eta^2 = 0.23$; Figure S3) and the interaction term (Wilks partial $\eta^2 = 0.19$; Figure 2C). At the univariate level of the trait, the *ecotype* effect size was larger than both the pair (Figure S3) and interaction term (Figure 2C) for most traits (i.e., more data points above the dotted line than below, see Table S4 for details). The larger effect sizes for the ecotype terms suggest that the phenotypic variation within the system is mainly explained by differences between ecotypes rather than replicate pairs, suggesting that broad-sense phenotypic differences between ecotypes might predominate over narrow-sense in *S. lautus*.

Broad-sense phenotypic parallelism

Parallel ecotype. We found striking differences between the mean Dune and Headland phenotypes for both plant architecture and leaf characteristics (illustrated in Figure 2D). In multivariate space, Dune and Headland ecotypes clearly clustered into two distinct groups (Figure 2E; Pillai's Trace = 0.73, $F_{1, 603} = 175.13$, $P < 2.2 \times 10^{-16}$). This pattern held true when traits were separated into plant architecture (Figure S2A; Pillai's Trace = 0.63, $F_{1, 603} = 202.42$, $P < 2.2 \times 10^{-16}$) and leaf categories (Figure S2B; Pillai's Trace = 0.61, $F_{1, 603} = 233.15$, $P < 2.2 \times 10^{-16}$). Across all traits, K-means clustering analysis correctly assigned 95% of Dune individuals, and 87% of Headland individuals into the correct cluster, further suggesting the majority of individuals within an ecotype are more phenotypically similar than between ecotypes. When traits were split into plant architecture and leaf, these numbers were slightly reduced. For plant architecture traits alone, 91% of Dunes and 82% of Headlands were assigned to the correct cluster. For leaf traits, 93% of Dunes and 78% of Headlands were correctly assigned.

We performed a linear discriminant analysis (LDA) on all traits to ask which linear combination of traits best explains the phenotypic differences between Dune and Headland ecotypes. The LDA was strongly loaded by leaf area and secondary branch angle, followed

by leaf dissection, leaf circularity, and widest width of the plant (Figure 3C). All traits were loaded in the same direction, except for widest width, leaf dissection, and leaf circularity. The LDA suggests that divergence between ecotypes is multivariate and has occurred on the majority of measured traits, and that a single trait does not dominate the phenotypic differences between ecotypes.

Parallel trait. We first used vote-counting to quantify whether the traits in the Dune and Headland populations of each pair have evolved in the same direction. For all traits, at least six of the eight pairs evolved in parallel (Figure 3A). Four of the nine traits had all eight pairs evolving in the same direction (S-statistic = 8, P = 0.0078), and three traits had seven pairs evolving in the same direction (S-statistic = 7, P = 0.035). Trait-by-trait linear models revealed a significant main effect of ecotype for each trait (Table S4), suggesting there are differences between Dune and Headland populations for all traits. The proportion of phenotypic variance explained by the ecotype term (R^2) for linear models with population means revealed six strongly parallel traits ($R^2 \geq 0.50$), one moderately parallel trait ($0.50 > R^2 \geq 0.33$), and two weakly parallel traits ($R^2 < 0.33$; Figure 3B). Five traits (vegetative height, main stem diameter, secondary branch angle, leaf area and leaf elongation) were consistently identified as parallel across each of the three approaches, three traits (widest width, main stem angle and leaf circularity) were parallel using two of the approaches, and one trait (leaf dissection) was parallel using only one approach (see Table S5 for more details).

Overall, we observed strong broad-sense phenotypic parallelism within *S. lautus* at the level of both the ecotype and trait. To address whether each replicate pair is phenotypically similar, we next asked whether the phenotypic differences between Dune and Headlands were consistent across replicate pairs.

Narrow-sense phenotypic parallelism

Parallel pair. We used Phenotypic Change Vector Analysis (PCVA) to ask how parallel each replicate pair is in terms of both the magnitude of divergence, and the contribution of traits to that divergence. Within multivariate phenotypic space, there were different levels of divergence (ΔL) between replicate pairs (Figures 4A, 4B). Considering all traits, the mean ΔL ($\pm$SE) between pairs was 1.7 ± 0.15. Out of the 28 pairwise comparisons, we only observed nine statistically parallel comparisons (i.e., $\Delta L \approx 0$; 32.1% of pairwise comparisons; Table S6). Therefore, most population pairs have different amounts of divergence between the

Dune and Headland populations. When we separately analyzed traits as two categories (plant architecture and leaf shape), we captured a signal of parallel divergence across a greater number of replicate pairs (Figures S4, S5). We observed ten statistically parallel comparisons for plant architecture traits (mean ΔL 1.0 ± 0.12; Table S7), and thirteen statistically parallel comparisons for leaf traits (mean ΔL 0.93 ± 0.14; Table S8).

The contribution of traits to divergence (θ) was quite variable across pairs (Figures 4A, 4C). Out of the 28 pairwise comparisons, only one angle was parallel, i.e., $\theta \approx 0°$ (3.6% of pairwise comparisons; Table S9), indicating that a different contribution of traits is involved in the divergence between most pairs. The mean angle (±SE) between population pairs was 39.5 ± 2.1°; all angles were acute, with a maximum of 62.8°. When traits were split into plant architecture and leaf categories, we again captured a stronger signal of phenotypic parallelism for both categories. We observed nine statistically parallel angles for plant architecture traits (mean angle 29.8 ± 3.0°; Table S10) and four statistically parallel for leaf traits (42.6 ± 3.4°; Table S11).

Overall, narrow-sense phenotypic parallelism (i.e., the similarities between replicate pairs) was weak within the system. Most pairs had different magnitudes of divergence (ΔL), with different contribution of traits to divergence (θ).

Broad-sense genotypic parallelism

Parallel nucleotide site. The relative contributions of broad- and narrow-sense parallelism revealed that very few sampled SNPs explained more variance between ecotypes than between pairs (Figures 5A, 5C, S6A, S6C). Specifically, only 6.3% of sampled SNPs contained a partial effect size of the ecotype term that was larger than the interaction term (i.e., those above the dashed line in Figure 5A which are also > 0 in Figure 5C). This dramatically decreases to 0.68% when we only consider SNPs with partial effect sizes > 0.1. This indicates that parallel evolution at the level of the nucleotide site within the system is largely predominated by differences between replicate pairs, suggesting that adaptation in each pair is occurring via different SNPs.

We identified 93 sites that were highly differentiated between Dune and Headland populations (~1% of sequenced SNPs). These SNPs were considered broad-sense outliers comparing all Dune vs all Headland populations (approach 1). Fifty-four of the 93 SNPs fall

within genic regions, whereas 39 are in non-genic regions. However, we must note our GBS data is biased towards genic regions (due to the enzymes preferentially cutting within gene-rich regions). When considering outliers detected within each replicate pair that contained concordant allele frequency differences across pairs (approach 2), we detected 15 parallel nucleotide sites (0.16% of SNPs; Figure S7). These 15 SNPs had concordant allele frequency differences in either all nine (S-statistic = 9, P = 0.004), or eight (S-statistic = 8, P = 0.04) replicate pairs. Nine of these SNPs fall within genic regions, whereas six are in non-genic regions. Five SNPs were detected as outliers in both approaches (three genic, two non-genic; Figure 6A; red dots in Figure 5A). These five nucleotide sites are considered the best candidates for broad-sense parallelism as they show both high differentiation between ecotypes, with concordant allele frequency changes in each replicate pair. The average difference in allele frequency between Dune and Headlands for the three genic SNPs was 0.55 (SD = 0.096), whereas the average for the two non-genic SNPs was 0.57 (SD = 0.107). See Figure S8 for a summary of broad-sense phenotypic parallelism at the level of the nucleotide site.

Parallel gene. The relative contributions of broad- and narrow-sense parallelism at the level of the gene revealed that very few genes explained more variance between ecotypes than between pairs (Figures 5B, 5D, S6B, S6D). More specifically, only 6.3% of SNPs contained a partial effect size of the ecotype term that was larger than the interaction term (i.e., those above the dashed line in Figure 5A which are > 0 in Figure 5C). Although this number dramatically decreases to 1.4% when we only consider genes which have a partial effect sizes > 0.1. This indicates that differences between replicate pairs largely predominates parallel evolution at the level of the gene within the system, suggesting that adaptation in each pair is likely occurring at different genes.

Of the five candidate outlier SNPs identified above using the outlier approach (i.e., those showing high differentiation between ecotypes in approach 1 and also concordant allele frequency chances across replicate pairs in approach 2), the three genic SNPs fall within three separate genes, two of which have homologs within *Arabidopsis* (Appendix S1; red dots in Figure 5B). These two genes encode a galactose oxidase/kelch repeat superfamily protein (*AT5G04420*; Figure 6A first panel) and a basic salivary proline-rich-like protein (*AT5G14540*; Figure 6A last panel). The proteins are both located in the cytosol and are both widely expressed in structures including the leaves, stem, reproductive organs, roots, and

seeds (Klepikova *et al.*, 2016). Considering approach 1 and 2 separately, the 54 outlier genic SNPs detected in approach 1 fall in 49 separate genes, of which 48 have homologs within *Arabidopsis*. The majority of these genes have functions in the nucleus, cytoplasm, plasma membrane, mitochondria and chloroplast, and are involved in processes including ion transport, transcription, response to heat, response to water deprivation, DNA repair and embryo development (see Appendix S1 for details of each gene). For approach 2, the nine outlier genic SNPs from approach 2 fall in nine separate genes, of which seven have homologs within *Arabidopsis*. These genes have functions in the nucleus, cytoplasm, plasma membrane and mitochondria, and are involved in processes including ion transport, aminoacylation, embryo development and DNA repair (see Appendix S1 for details of each gene). See Figure S8 for a summary of broad-sense phenotypic parallelism at the level of the gene.

Parallel biological function. Because we only sampled two candidate broad-sense outlier genes that had predicted proteins, we did not perform an enrichment analysis on them. However, we performed enrichment analysis on 1) the 54 genes from approach 1 (of which 48 contained *Arabidopsis* protein homologs), and 2) the nine genes from approach 2 (of which seven contained *Arabidopsis* protein homologs). For approach one, the category of *helicases* (UniProtKB keywords) was significantly enriched ($P = 0.0344$; P-value is the EASE score, a modified Fisher Exact P-value). When using the more stringent approach by considering clusters to be enriched if Benjimani-adjusted $P < 0.05$ and $FRD < 1$, there were no enriched categories. The functions of the genes within this helicase category are involved in DNA replication, recombination and repair, and often associated with tolerance to drought and salinity in plants (Owttrim, 2006). There were no significantly enriched functions with approach 2.

Narrow-sense genotypic parallelism

Parallel nucleotide site. We detected highly differentiated nucleotide sites (i.e., outliers) between the Dune and Headland of each locality (i.e., for each replicate pair), and compared how many outlier SNPs were common between all pairwise comparisons of replicate pairs. On average, 157 outlier SNPs (SD = 74.5) were shared between two replicate pairs, and for each pairwise comparison the shared SNPs were greater than expected by chance (Table S12), This suggests some degree of narrow-sense parallelism at the level of the nucleotide site. We detected six nucleotide sites that were outliers in seven pairs (Figure 6B), however,

639 there were no outlier SNPs common to all nine pairs, suggesting that even though there are
640 common outliers between individual pairs, this does not translate to common outliers across
641 the system as a whole. This is because within narrow-sense genotypic parallelism, a parallel
642 nucleotide site across all pairs has to be separately detected as an outlier in each replicate
643 pair. Conversely, a broad-sense outlier may reflect strong ecotypic differentiation even if
644 some nucleotide sites are not statistical outliers in every replicate pair.

645 **Parallel gene.** We detected highly differentiated genes between the Dune and Headland of
646 each locality (i.e., for each replicate pair), and compared how many of these outlier genes
647 were common between all pairwise comparisons of replicate pairs. On average, 124 outlier
648 genes (SD = 54.6) were shared between two replicate pairs. The shared outlier genes between
649 all pairwise comparisons were greater than expected by chance, except for one comparison
650 (D14-H15 vs D32-H12; Table S13). Thirty-nine genes were outliers in at least eight or nine
651 replicate pairs (Figure 6B), of which 36 contained homologs in *Arabidopsis*. These genes
652 have functions in the nucleus, cytoplasm, plasma membrane, chloroplast, vacuole and
653 endoplasmic reticulum, and are involved in processes including ion transport, transcription,
654 seed development, response to auxin, response to heat, response to salt stress, embryo
655 development and cell growth (see Appendix S1 for details on each gene).

656 **Parallel biological function.** For each replicate pair we conducted a gene-enrichment
657 analysis using outlier genes to ask whether any biological functions were enriched and
658 whether the same functions were repeatedly enriched across replicate pairs. Across all pairs
659 there were 17 enriched functions (Figure 6C; Table S14). No function was repeatedly
660 enriched in all nine replicate pairs, although two functions (*chloroplast* and *nucleotide-*
661 *binding/ATP-binding;* UniProtKB keywords) were enriched across eight replicate pairs, this
662 being greater than expected by chance (S-statistic = 8, P = 0.04).

663 Within the *chloroplast* category, the majority of outlier genes across pairs have functions in
664 the chloroplast, cytosol, mitochondria, nucleus, vacuole and the cell wall, and are involved in
665 processes including oxidation reduction, response to light, translation, proteolysis, protein
666 phosphorylation and protein folding. See Appendix S2 for details on each gene within the
667 *chloroplast* category and the number of replicate pairs the genes were detected as an outlier.
668 This *chloroplast* category also contains three genes that encode for ABCB proteins
669 (ABCB19, ABCB20, ABCB21, which are outliers in at least four replicate population pairs).
670 ABCBs function in transporting the hormone auxin, which regulates plant growth and

development (Cho & Cho, 2013). Auxin plays a key role in a plants ability to respond to gravity (Strohm *et al.*, 2012), and seems to be a largely responsible for the overall prostrate and erect phenotypes within the system (Wilkinson *et al.*, 2020). Within the *nucleotide-binding/ATP-binding* category, the majority of outlier genes across pairs have functions in the chloroplast, nucleus, plasma membrane, cytosol, mitochondria, cytoplasm, and are involved in processes including protein phosphorylation, protein folding, transcription, aminoacylation, ion transport, and response to stress. See Appendix S3 for details on each gene within the *nucleotide/ATP-binding* category and the number of replicate pairs the genes were detected as an outlier.

Across the nine replicate pairs, the distribution of the proportion of shared outlier nucleotide sites was significantly different to the outlier genes ($X^2 = 279.65$, df = 8, $P < 2.2x10^{-16}$), and biological functions ($X^2 = 361.95$, df = 8, $P < 2.2x10^{-16}$). The distributions of the genes and biological functions were not significantly different across the nine replicate pairs ($X^2=14.52$, df=8, P = 0.069). When using the more stringent approach by considering clusters to be enriched if Benjimani-adjusted $P < 0.05$ and the False Discovery Rate < 1, the two functional categories that were enriched across the most number of replicate pairs were still the *chloroplast* category and the *nucleotide-binding/ATP-binding* category (Table S15), suggesting these results are quite robust.

Variation in phenotypic parallelism

Gene flow did not constrain phenotypic divergence, as there was no relationship between levels of gene flow and the lengths of phenotypic vectors (L) between ecotypes within a locality for the Dune to Headland gene flow ($F_{1,6} = 0.007$, P = 0.934, $R^2 = 0.001$), Headland to Dune gene flow ($F_{1,6} = 1.17$, P = 0.321, $R^2 = 0.163$), or absolute gene flow ($F_{1,6} = 0.061$, P = 0.463, $R^2 = 0.092$). There was also no relationship between divergence time between ecotypes and L within a locality ($F_{1,6} = 0.321$, P = 0.592, $R^2 = 0.051$). Environmental distance did not relate to how phenotypically divergent (θ) a population pair was ($F_{1,3} = 0.046$, P = 0.843, $R^2 = 0.015$), although we treat these data with caution due to low sample size of the environmental data (as environmental data were only available for five localities). Population pairs that were more phenotypically similar (i.e., smaller ΔL) did not share more outlier SNPs, genes or biological functions (Mantel test SNPs: r = -0.215, P = 0.894; Mantel test genes: r = -0.164, P = 0.835, Mantel test biological functions: r = -0.179, P = 0.837). Population pairs with similar contribution of traits to divergence (i.e., smaller θ) also did not

share more outlier SNPs, genes, or biological functions (Mantel test SNPs: r = -0.493, P = 0.989; Mantel test genes: r = -0.347, P = 0.865; Mantel test biological functions: r = -0.337, P = 0.93).

Discussion

We have developed an integrative framework to measure parallel evolution at the phenotypic and genotypic levels. Our approach aims to quantity the overall variation between ecotypes (broad-sense parallelism) as well as the variation between replicate population pairs (narrow-sense parallelism). Applying our framework to *Senecio lautus*, we have demonstrated that the independent adaptation of populations to dune and headland environments has resulted in the repeated evolution of similar phenotypes. In each replicate population, these ecotypes have mainly diverged via different mutational changes in different genes, though some of these belong to the same predicted biological function. These results add further adding credence to the notion of independent ecotypic differentiation along the Australian coast. In particular, they are consistent with 1) the demographic history of the system detailed in James *et al.*, (2020), which showed that the evolution of each population is highly independent due to strong isolation by distance, and 2) the observation of strong local adaptation measured in multiple reciprocal transplant experiments in the system (Melo *et al.*, 2014; Richards *et al.*, 2016; Richards & Ortiz-Barrientos, 2016; Walter *et al.*, 2016, 2018b; Wilkinson *et al.*, 2020). Below we discuss the framework we proposed to understand parallel evolution in light of *S. lautus* and consider how the genetics and ecology of these coastal ecotypes impact the likelihood of phenotypic and genotypic parallelism. We finish by discussing when our framework should be used, address its potential caveats, and how it could contribute to future studies of parallel evolution in nature.

Phenotypic parallelism

In *S. lautus*, the phenotypic differences between ecotypes were greater than the variation arising from replicate pairs in both multivariate and univariate space. For instance, the partial effect size of the ecotype was 86% for multivariate phenotypic differences, whereas the partial effect size of replicate pairs was only 19%. This was also true for most traits when considered alone, where ecotypic differences explained most variation in vegetative height, the angle of secondary branches, and the size of leaves. These traits largely capture the overall growth habits of the two ecotypes: prostrate and erect. Partitioning variance between

734 ecotypes and replicate pairs can indicate the relative contributions of broad- versus narrow-
735 sense parallelism and in this case, it reveals broad-sense phenotypic parallelism is likely very
736 strong in the *S. lautus* system. To see this in greater detail, we now discuss results from our
737 other analyses of broad-sense parallelism in *S. lautus* and compare them to other systems of
738 parallel evolution.

739 Broad-sense phenotypic parallelism (i.e., the net contribution of all independent replicate
740 populations within each ecotype to the overall phenotypic differences between ecotypes) was
741 strong in the coastal Dune and Headland ecotypes. At the level of the ecotype we observed
742 striking phenotypic differences between ecotypes in multivariate trait space, with little
743 overlap between ecotypes. This strong broad-sense phenotypic parallelism is seen in other
744 empirical parallel evolution systems such as lake-stream stickleback on Haida Gwaii in
745 Canada (Deagle *et al.*, 2012), and dwarf-normal lake whitefish (Laporte *et al.*, 2015), where
746 there is a clear phenotypic separation of ecotypes in the first two dimensions of multivariate
747 space. In contrast, some systems of parallel evolution have lower broad-sense phenotypic
748 parallelism, where there is overlap between ecotypes in phenotypic space. For instance,
749 benthivorous-planktivorous Arctic charr (Jacobs *et al.*, 2020), benthic-limnetic cichlid fishes
750 (Elmer *et al.*, 2014) and lake-stream stickleback on Vancouver Island in Canada (Stuart *et al.*,
751 2017) do not have each ecotype occupying a separate region in the first two dimensions of
752 multivariate space, thus likely having lower broad-sense phenotypic parallelism. (Note that
753 some overlap in multivariate variance can still lead to significant broad-sense parallelism.)

754 Broad-sense phenotypic parallelism at the level of the trait was high in *S. lautus*. This was
755 true for all measured traits, except for leaf dissections, which seem to vary more between
756 replicate pairs than between ecotypes. This pattern is rather different to other systems where
757 the contribution of traits to ecotypic differences has been calculated. For instance in
758 stickleback ecotypes, Stuart *et al.*, (2017) found that the variation in most traits is explained
759 mainly by differences between replicate pairs rather than between ecotypes, suggesting little
760 parallelism at the level of individual traits. This discrepancy might disappear if more traits are
761 measured in *S. lautus*, but the phenotypic dimensionality of the system does not seem to be
762 very high: of the 14 traits we measured, we discarded five highly correlated traits. In other
763 studies of *S. lautus* where more traits have been measured (Walter *et al.*, 2018a), strong
764 genetic correlations exist amongst a variety of vegetative traits suggesting strong
765 interdependence between morphological modules such as leaf and plant architecture.

In contrast, narrow-sense phenotypic parallelism (i.e., the similarities between replicate population pairs, quantified with PCVA) in *S. lautus* was weak, with most pairs having different magnitudes of divergence (32.1% of pairwise comparisons were parallel, i.e., $\Delta L \approx 0$) and different contribution of traits to divergence (3.6% of pairwise comparisons were parallel, i.e., $\theta \approx 0°$). Although the PCVA approach is relatively new within studies of parallel evolution, a recent study in 16 lake-stream stickleback pairs discovered even less narrow-sense parallelism than *S. lautus*, with 27.5% of pairwise comparisons having parallel magnitudes of divergence, and only 0.83% of pairwise comparisons with parallel contribution of traits to divergence (Stuart *et al.*, 2017). As more systems adopt the PCVA approach we will be able to directly compare the amount of parallelism between replicate populations across different study systems, although the creation of null distributions for the process remains unexplored.

One interpretation for the strong broad-sense and weaker narrow-sense phenotypic parallelism in *S. lautus* comes when considering the nature of the phenotypic and fitness landscapes. Our current work has revealed that the Dunes and Headlands are quite phenotypically distinct, yet there are still phenotypic differences between the populations within each ecotype, which seem to be more pronounced in the Headlands (the phenotypic centroids of Dune populations cluster, but Headland populations are somewhat more scattered in multivariate space). Furthermore, previous reciprocal transplant experiments in *S. lautus* have demonstrated that ecotypes are locally adapted and exhibit a strong reduction in fitness when grown in foreign habitats (Melo *et al.*, 2014; Richards *et al.*, 2016; Richards & Ortiz-Barrientos, 2016; Walter *et al.*, 2016, 2018b; Wilkinson *et al.*, 2020). This suggests that Dune and Headland ecotypes reside on quite distinct regions of the fitness landscape. Previous work has also shown that Dune individuals are equally fit across other non-local sand dune habitats. This suggests that the fitness landscape for the Dunes might share a common optimum. On the other hand, Headland individuals have reduced fitness in non-local headland habitats (Walter *et al.*, 2016), which implies some environmental heterogeneity within rock headlands (Roda *et al.*, 2013b). Therefore, the fitness landscape for Headlands might be either more broad and rugged, or with multiple optima, with each Headland population residing on a different local optimum. Overall, these differences in phenotypic variance within each ecotype some may explain why narrow-sense phenotypic parallelism is low in *S. lautus*.

Finally, the nature of parallelism in a system can depend on the nature of selection driving adaptation and on whether selection drives the evolution of one or multiple traits. For instance, ecotypic description of systems, such as sticklebacks and cichlids, is often binary and relies on correlating a large environmental category to a general perception of the phenotypic differences between populations. In *S. lautus*, Dune and Headland ecotypes are qualitatively different in their growth habit, where Dune individuals grow erect and tall, and Headland individuals grow prostrate forming mats over the ground. However, many traits seem to contribute simultaneously to the qualitative descriptions of prostrate and erect (Walter *et al.*, 2018a), suggesting that parallel evolution relies on coordinated trait evolution for size and for shape. In sticklebacks, on the other hand, only a few traits seem to be highly parallel across replicate pairs (Stuart *et al.*, 2017). One simple explanation for these discrepancies is that parallel evolution may rely mostly on the origin of either complex or simple adaptations, and that it may involve either few genes of large effect (e.g., the *Eda* gene in sticklebacks; Colosimo *et al.*, 2005) or many of small effect, which is likely common during polygenic adaptation (Yeaman, 2015). Our genotypic results help shed some light on these different explanations for patterns of phenotypic parallelism in *S. lautus*.

Genotypic parallelism

Within *S. lautus*, the relative contributions of broad- and narrow-sense genotypic parallelism revealed that very few nucleotide sites and genes explained more variance between ecotypes than between pairs. This suggests there is little broad-sense genotypic parallelism within the system, where divergence is explained by differences between replicate pairs at the level of the nucleotide site and gene. This is also evident when detecting outliers between the ecotypes (i.e., the genetic differences between all Dune vs all Headland individuals), where very few nucleotide sites and genes distinguished the ecotypes. Narrow-sense genotypic parallelism within the system (i.e., the genetic similarities between Dune-Headland replicate pairs) was strongest at the level of the biological function, although there was some sharing of common outlier nucleotide sites and genes across replicate population pairs. These results suggest that adaptation in *S. lautus* could be rather flexible and redundant at lower levels of organization (the nucleotide site and gene), and only parallel at the level of the biological function. Parallelism at the biological function level might be common within nature (e.g., Smith & Rausher, 2011; Kowalko *et al.*, 2013; Roda *et al.*, 2013b; Laporte *et al.*, 2015; Perreault-Payette *et al.*, 2017; Cassin-Sackett *et al.*, 2019) given that there are fewer

biological functions than there are genes or nucleotide sites (Tenaillon *et al.*, 2012; Tiffin & Ross-Ibarra, 2014). In this regard, our study is rather conservative as we have only defined narrow-sense parallelism in function when the function was separately enriched in at least all nine, or eight population pairs. Even in those few enriched functions, the set of sequenced genes that were divergent in each population pair were often different (Tables S16, S17), further suggesting that adaptation in *S. lautus* might be quite robust and is possibly underpinned by polygenic adaptation and functional redundancy of alleles at different loci (Barghi *et al.*, 2020).

Recent studies in this system have demonstrated that hormone signaling, specifically the auxin pathway, is divergent between Dune and Headland populations (Roda *et al.*, 2013b; Wilkinson *et al.*, 2020). This indicates that integrated and modular phenotypes might be key to the patterns of parallel evolution we have observed at the genotypic level in this system. We therefore expected to find highly differentiated auxin-related genes within our current study. Consistent with this prediction, we detected divergent genes involved in the auxin pathway that are differentiated across multiple population pairs, including GH3.1 (Staswick *et al.*, 2005), NPH4 (Harper *et al.*, 2000) and genes from the ABCB family (Cho & Cho, 2013), see Appendix S4 for more details. This gives further evidence that auxin may play a key role in creating the contrasting prostrate and erect phenotypes in *S. lautus*. Future studies on the molecular basis of adaptation should focus on the concomitant contribution of many genes to phenotypic variation and to their shared cellular and physiological roles, as it is likely that variation in regulatory networks might underlie a large fraction of the adaptive space in organisms (Boyle *et al.*, 2017; VanWallendael *et al.*, 2019).

The demographic history of species can also alter the patterns of genotypic parallelism (Conte *et al.*, 2012; Ord & Summers, 2015). The most trivial reason is the contribution of drift to diversity and divergence, particularly when populations are sufficiently small. In such scenarios, not surprisingly, many outlier loci can stochastically increase in frequency in each population pair, thus reducing levels of both broad- and narrow-sense genotypic parallelism. This is one argument for grouping outliers through their cellular and physiological function, as drift will be less likely to create functional similarities across population pairs. Future studies of parallelism should not only identify outlier loci that are unlikely to have drifted to fixation, but also ask if they have functional relationships amongst them. Although more challenging, identifying loci with concordant patterns of divergence, even if they are not

outliers *per se*, can also reveal sets of genes that contribute to consistent patterns of divergence across populations and that are thus likely to be responsible for polygenic signatures of adaptation (Berg & Coop, 2014; Tiffin & Ross-Ibarra, 2014; Barghi *et al.*, 2020).

Broad- and narrow-sense parallel evolution framework

Within the literature, the debate surrounding the term parallel evolution manifests because parallelism can arise at different scales of phenotypic and genotypic divergence, as well as different genetic levels of biological organization. Here, our framework proposes to categorize parallel evolution into the broad- and narrow-sense scales (at both the phenotypic and genotypic levels) to help quantify both the overall patterns between ecotypes, as well as the similarities of each replicate pair. We suggest that researchers need to be explicit when referring to either phenotypic or genotypic patterns of parallelism, whether these patterns exist across the system as a whole, or only between particular replicate pairs, and at what level of biological organization the genotypic parallelism occurs (i.e., nucleotide site, gene or biological function).

A 'perfectly' parallel system at the level of the phenotype would contain distant phenotypic differences between ecotypes (i.e., strong broad-sense phenotypic parallelism), with replicate pairs that are effectively identical in their phenotypic differences (i.e., strong narrow-sense phenotypic parallelism). Such a system would imply that evolution is extremely repeatable and predicable at the level of the phenotype (Blount *et al.*, 2018), where every instance of repeated evolution has resulted in the same phenotypic adaptations. However, this may be highly unlikely within natural systems due to a range of factors such as environmental heterogeneity within each habitat, the interplay between the genotype, phenotype and fitness landscapes, genetic constraints, and stochastic forces such as genetic drift (Lenormand *et al.*, 2009, 2016; Rosenblum *et al.*, 2014; Fraïsse & Welch, 2019).

A 'perfectly' parallel system at the level of the genotype would show the same nucleotide sites involved in adaptation across replicate pairs, with evidence that the mutation(s) have undergone repeated and independent selection in each population. Again, this may be highly unlikely within natural systems, especially in systems with phenotypic redundancy (with many phenotypic solutions to the same problem), and when adaptive traits are polygenic (Yeaman, 2015). Also, the likelihood of genetic parallelism at the nucleotide site is highly

dependent on the availability of adaptive mutations (Chevin *et al.*, 2010; Ralph & Coop, 2010; Stoltzfus & McCandlish, 2017; Bailey *et al.*, 2018). Within genotypic parallelism, the nested levels of biological organization imply that parallelism at the lowest level (i.e., the nucleotide site) will translate to parallelism at the gene and biological function levels. We therefore must keep in mind that when parallelism occurs at a given level (i.e., the biological function), it will not necessarily occur at levels below (i.e., the gene and nucleotide site).

The effects of sampling on parallelism

The ability to detect genotypic parallelism is impacted by sampling. Obvious pitfalls exist for methods that do not sample the entire genome. For instance, reduced representation libraries sparsely sample the genome, and tend to be biased towards non-genic regions (Lowry *et al.*, 2017). Although we by-pass this problem to some extent as our enzyme cuts disproportionally gene rich regions of the genome (~60-70% of RAD loci map to the transcriptome of *S. lautus*), sequencing of reduced representation libraries will likely fail to sample many loci involved in adaptation (Tiffin & Ross-Ibarra, 2014; Lowry *et al.*, 2017). Even sequencing of whole genomes might still fail to sample adaptive loci due to the lack of sequencing of important regions. In addition, the effects of recombination (Booker *et al.*, 2020), background selection, linkage and demography affects the distribution of F_{ST} throughout the genome and impacts our ability to detect regions involved in adaptation (see Hoban *et al.*, 2016 for a review).

Additionally, common F_{ST} -based approaches, including those used within this study can fail to detect other structural aspects of the genome that can be involved in adaptation (Wellenreuther *et al.*, 2019), including copy number variation (Schrider *et al.*, 2016; Nelson *et al.*, 2019), local recombination rate variation (Reeve *et al.*, 2016; Ortiz-Barrientos & James, 2017; Samuk *et al.*, 2020), inversions (Kirkpatrick & Barton, 2006; Lowry & Willis, 2010; Faria *et al.*, 2019), and transposons (González & Petrov, 2009; Schrader & Schmitz, 2019). Furthermore, the alleles contributing to adaptation are also difficult to detect if adaptation has proceeded by many alleles of small effect, which may be quite common in highly polygenic traits (Yeaman, 2015). In such systems, divergent loci are difficult to detect as they contain low F_{ST}, which further makes detecting genetic parallelism highly unlikely in these systems. Finally, traditional approaches that sample SNPs across the genome will fail to detect variation in gene expression levels, which may also be involved in adaptation during parallel evolution (e.g., Rivas *et al.*, 2018; Verta & Jones, 2019).

The quantification of phenotypes may also experience sampling bias. We may be unknowingly biased towards measuring traits that are divergent between ecotypes, rather than the overall phenotype of an organism. We might also overlook parallelism in traits we did not measure, such as adaptive phenotypes like flowering time in plants (Blackman *et al.*, 2011; Christie & Strauss, 2019), or disregard traits that would be difficult to measure (such as the root networks of plants), or physiological responses to a stimulus (such as tropisms in plants). Although these traits might be highly correlated to other measured traits, especially for highly modular phenotypes (Murren, 2012), this needs to be first demonstrated experimentally before deciding which traits to measure and which traits to disregard. We must therefore be aware that the likelihood of detecting parallelism is highly dependent on the type and number of traits measured in a system (Stayton, 2008), suggesting that further work needs to enrich current theories of multi-trait evolution so we can develop better null hypotheses for parallel evolution while accounting for correlations between traits, including those that are highly pleiotropic (Yeaman, 2015; De Lisle & Bolnick, 2020).

The geometry and statistics of parallel evolution

When quantifying narrow-sense phenotypic parallelism with vectors, the interpretation of phenotypic change in lengths (ΔL) and angles (θ) between replicate population pairs should be treated with caution. This is due to how phenotypic similarities manifest both within each replicate pair and between ecotypes. Consider two replicate pairs where the populations within each pair are more phenotypically similar than the populations belonging to the same ecotype (i.e., they had different common ancestors; Bolnick *et al.*, 2018). However, due to their phenotypic configuration in multivariate space, we may still measure the same change in length ($\Delta L \approx 0$) and angle ($\theta \approx 0°$) between pairs. This is apparent in the work by Elmer *et al.*, (2014), where they showed strong ecological parallelism in two replicate limnetic-benthic cichlid replicate pairs, despite the phenotypic differences being larger between pairs than between ecotypes within a pair. This highlights that systems with weak broad-sense phenotypic parallelism but strong narrow-sense, might be describing a type of parallel evolution where replicate populations have adapted to similar environmental challenges via different phenotypic changes but through functionally equivalent evolution. In our work we have found a striking case of strong phenotypic differences between Dune and Headland *S. lautus* ecotypes despite variable levels of narrow-sense parallelism. Further investigation of

other biological axes of organization will further complement our current view of this system, such as the contributions of physiology and network evolution to adaptation and divergence.

Comparing levels of parallel evolution across systems

To advance the field of parallel evolution, it is necessary to undertake statistical approaches that allow us to compare levels of parallelism across systems on a common scale. It would also be useful to have key criteria to define the amount of parallelism in a system. Rather than classifying evolution as 'parallel' or 'non-parallel,' we should strive to place each system on a continuum of parallelism, as suggested by the recent work by Bolnick *et al.*, (2018) which discusses the (non)-parallel continuum. Our framework attempts to clarify the continuum of parallel evolution into broad- and narrow-sense scales at both the genotypic and phenotypic levels, thus paving the way for finding common ground in conceptualizing and measuring parallel evolution across systems.

One potential way forward to compare between systems is to use variance partitioning methods (such as partial effect sizes; partial η^2) to gain an overall understanding of the relative contributions of broad- and narrow-sense parallelism. This can be undertaken at the multivariate and univariate levels of the phenotype as well as the level of the SNP and gene for the genotype. We can then compare the distribution of effect sizes at these different levels across study systems. Systems that have more broad-sense parallelism will show a larger proportion of partial effect sizes (either at the phenotypic or genotypic level) where the variance is explained by differences between the ecotypes rather than replicate pairs. Researchers may also benefit from approaches such as the K-means clustering analysis, where we can directly compare the percentage of individuals correctly assigned to each ecotype (also see the work on exchangeability by Hendry *et al.*, 2013). For instance, for a system with high broad-sense phenotypic parallelism at the level of the ecotype, we would be able to easily predict which ecotype all individuals belong, based on their phenotypic traits.

Recent work by De Lisle & Bolnick (2020) advocates the use of theory from quantitative genetics to quantify the direction of evolutionary change in multivariate space across systems of parallel evolution. It has some advantages over the PCVA approach as rather than interpreting individual vectors and angles, it uses the full matrix of correlations between populations and asks which dimensions of multivariate space explain a significant amount of variance. One can then extract the loadings from these dimensions to quantify the

combination of traits that contribute to the divergence between populations. Parallelism can be assessed by asking whether the loadings are in the same direction across replicate populations. Similar quantitative genetics approaches (McGuigan, 2006) have been used in multiple systems to quantify phenotypic and genetic divergence between populations (e.g., McGuigan *et al.*, 2005; Chenoweth *et al.*, 2010). Within the *S. lautus* system, multivariate divergence between ecotypes and its association with the additive genetic variance underlying phenotypic traits suggests that Headland populations have strong phenotypic constraint arising from strong genetic correlations whereas Dune populations are freer to evolve across many axes of genetic variance (Walter *et al.*, 2018a). This approach, now extended by De Lisle & Bolnick (2020) to also generate null hypotheses, promises to be a powerful approach to measure parallelism, but whether additive genetic variances can be measured in most systems remains a formidable challenge. Future work on null hypotheses should also strive to model the likelihood of phenotypic or genotypic parallelism while taking into account variance in factors such as gene flow, environmental heterogeneity, the recombination landscape, and the genetic architecture of adaptive traits (e.g., Thompson *et al.*, 2019).

To further advance the field of parallel evolution, researchers must also strive to specifically identify the causal genes for adaptation by directly linking them to adaptive phenotypes and further demonstrating that these phenotypes confer a fitness advantage to native populations. In systems where adaptation is governed by selection on the same nucleotide sites (e.g., Colosimo *et al.*, 2005), researchers must demonstrate whether the selected loci arose via standing genetic variation or new mutations (Lee & Coop, 2017, 2019). The field of parallel evolution also requires a more thorough understanding of how the demographic history of populations impacts the likelihood of genotypic and phenotypic parallelism (e.g., Bohutínská *et al.*, 2020). Furthermore, understanding the contributions of phenotypic plasticity within each system (by comparing natural populations to those reared in common garden conditions; Oke *et al.*, 2016) will help shed light on whether phenotypic parallelism is enhanced or dampened by non-genetic changes.

We have outlined a framework to quantify both phenotypic and genotypic parallel evolution within empirical systems. Applying this framework to *S. lautus*, we have demonstrated strong phenotypic differences between the Dune and Headland ecotypes, although most replicate pairs are slightly phenotypically different. Genotypic parallelism across pairs is mainly

driven by mutations in different genes, some of which belong to similar biological functions. Our work provides progress towards a common framework to measure and compare parallel evolution across natural systems.

Acknowledgements

We are grateful to H. N. Nguyen Vu for assisting with sample collection. We thank Ortiz-Barrientos laboratory members for insightful comments on previous versions of this manuscript. S. Chenoweth and M. Blows provided very useful feedback on M.E. James' PhD dissertation. This work was funded by The University of Queensland and the Australian Research Council grants to DO and JE, and by an Australian Postgraduate Award and a Graduate School International Travel Award to MEJ.

Author contributions

MEJ and DO conceived the project. MEJ, MW, HN and JE undertook sample collection and the field phenotypic measurements. MEJ extracted DNA, prepared libraries and performed bioinformatics. MEJ undertook all data analysis, and JE assisted with R code. MEJ and DO wrote the paper with input from all authors. DO is the mentor and supervisor for the research program.

Conflicts of interest

We do not have any conflicts of interest.

Data archival

Data will be uploaded to Dryad upon acceptance of the manuscript.

Appendices

Appendix S1. Broad- and narrow-sense outlier genes between replicate population pairs from coastal ecotypes of *S. lautus*

Functional annotation of the outlier genes within *DAVID*. Gene ontology is the *DAVID GOTERM_BP_DIRECT* (denoted below with *BP*), where absent, the *GOTERM_CC_DIRECT* was used (*CC*), and where absent, the *GOTERM_MF_DIRECT*

(*MF*) was used. *BS – A1* denotes genes detected as broad-sense outliers using approach 1 (see methods). *BS – A2* denotes genes detected as broad-sense outliers using approach 2. *NS* denotes genes detected in the narrow-sense that are common to either all nine (9) or eight (8) replicate pairs.

Appendix S2. Chloroplast outlier genes

Functional annotation of the outlier genes within the enriched biological function of 'chloroplast'. Gene ontology is the *DAVID GOTERM_BP_DIRECT* (denoted below with *BP*), and where absent, the *GOTERM_CC_DIRECT* was used (*CC*). *Number of replicate* pairs denotes how many replicate pairs the gene was detected as an outlier.

Appendix S3. Nucleotide-binding/ATP-binding outlier genes

Functional annotation of the outlier genes within the enriched biological function of 'nucleotide-binding/ATP-binding'. Gene ontology is the *DAVID GOTERM_BP_DIRECT* (denoted below with *BP*), and where absent, the *GOTERM_CC_DIRECT* was used (*CC*). *Number of replicate* pairs denotes how many replicate pairs the gene was detected as an outlier.

Appendix S4. Auxin-related outlier genes

Functional annotation of the outlier genes associated with the auxin pathway. Gene ontology is the *DAVID GOTERM_BP_DIRECT*. *Number of replicate* pairs denotes how many replicate pairs the gene was detected as an outlier.

References

Adams, D.C. & Collyer, M.L. 2009. A general framework for the analysis of phenotypic trajectories in evolutionary studies. *Evolution* **63**: 1143–1154.

Altschul, S.F., Gish, W., Miller, W., Myers, E.W. & Lipman, D.J. 1990. Basic local alignment search tool. *J. Mol. Biol.* **215**: 403–410.

Arendt, J. & Reznick, D. 2008. Convergence and parallelism reconsidered: what have we learned about the genetics of adaptation? *Trends Ecol. Evol.* **23**: 26–32.

Bailey, S.F., Guo, Q. & Bataillon, T. 2018. Identifying drivers of parallel evolution: A regression model approach. *Genome Biol. Evol.* **10**: 2801–2812.

Barghi, N., Hermisson, J. & Schlötterer, C. 2020. Polygenic adaptation: a unifying framework to understand positive selection. *Nat. Rev. Genet.*, doi: 10.1038/s41576-020-0250-z.

Berg, J.J. & Coop, G. 2014. A population genetic signal of polygenic adaptation. *PLoS Genet.* **10**: e1004412.

Bhatia, G., Patterson, N., Sankararaman, S. & Price, A.L. 2013. Estimating and interpreting FST: The impact of rare variants. *Genome Res.* **23**: 1514–1521.

Bierne, N., Gagnaire, P.A. & David, P. 2013. The geography of introgression in a patchy environment and the thorn in the side of ecological speciation. *Curr. Zool.* **59**: 72–86.

Blackman, B.K., Michaels, S.D. & Rieseberg, L.H. 2011. Connecting the sun to flowering in sunflower adaptation. *Mol. Ecol.* **20**: 3503–3512.

Blount, Z.D., Lenski, R.E. & Losos, J.B. 2018. Contingency and determinism in evolution: Replaying life's tape. *Science* **362**: eaam5979.

Bohutínská, M., Vlček, J., Yair, S., Laenen, B., Konečná, V., Fracassetti, M., *et al.* 2020. Genomic basis of parallel adaptation varies with divergence in *Arabidopsis* and its relatives. BioRxiv [Preprint]. https://doi.org/10.1101/2020.03.24.005397.

Bolnick, D.I., Barrett, R.D.H., Oke, K.B., Rennison, D.J. & Stuart, Y.E. 2018. (Non)Parallel evolution. *Annu. Rev. Ecol. Evol. Syst.* **49**: 303–330.

Booker, T.R., Yeaman, S. & Whitlock, M.C. 2020. Variation in recombination rate affects detection of outliers in genome scans under neutrality. BioRxiv [Preprint]. doi: https://doi.org/10.1101/2020.02.06.937813.

Boyle, E.A., Li, Y.I. & Pritchard, J.K. 2017. An expanded view of complex traits: From polygenic to omnigenic. *Cell* **169**: 1177–1186.

Broad Institute. 2019. *PicardTools*. Broad Institute, GitHub Repository. http://broadinstitute.github.io/picard/.

Butlin, R.K., Saura, M., Charrier, G., Jackson, B., André, C., Caballero, A., *et al.* 2014. Parallel evolution of local adaptation and reproductive isolation in the face of gene flow. *Evolution* **68**: 935–949.

Cai, Z., Zhou, L., Ren, N.N., Xu, X., Liu, R., Huang, L., *et al.* 2019. Parallel speciation of wild rice associated with habitat shifts. *Mol. Biol. Evol.* **36**: 875–889.

Cassin-Sackett, L., Callicrate, T.E. & Fleischer, R.C. 2019. Parallel evolution of gene classes, but not genes: Evidence from Hawai'ian honeycreeper populations exposed to avian malaria. *Mol. Ecol.* **28**: 568–583.

Catchen, J.M., Hohenlohe, P.A., Bernatchez, L., Funk, W.C., Andrews, K.R. & Allendorf, F.W. 2017. Unbroken: RADseq remains a powerful tool for understanding the genetics of adaptation in natural populations. *Mol. Ecol. Resour.* **17**: 362–365.

Chan, Y.F., Marks, M.E., Jones, F.C., Villarreal, G., Shapiro, M.D., Brady, S.D., *et al.* 2010. Adaptive evolution of pelvic reduction in sticklebacks by recurrent deletion of a Pitx1 enhancer. *Science* **327**: 302–305.

Chenoweth, S.F., Rundle, H.D. & Blows, M.W. 2010. The contribution of selection and genetic constraints to phenotypic divergence. *Am. Nat.* **175**: 186–196.

Chevin, L.M., Martin, G. & Lenormand, T. 2010. Fisher's model and the genomics of adaptation: restricted pleiotropy, heterogenous mutation, and parallel evolution: heterogeneous mutation effects across loci. *Evolution* **64**: 3213–3231.

Cho, M. & Cho, H. 2013. The function of ABCB transporters in auxin transport. *Plant Signal. Behav.* **8**: e22990.

Christie, K. & Strauss, S.Y. 2019. Reproductive isolation and the maintenance of species boundaries in two serpentine endemic Jewelflowers. *Evolution* **73**: 1375–1391.

Christin, P.A., Weinreich, D.M. & Besnard, G. 2010. Causes and evolutionary significance of genetic convergence. *Trends Genet.* **26**: 400–405.

Clarke, J.D. 2009. Cetyltrimethyl Ammonium Bromide (CTAB) DNA miniprep for plant DNA isolation. *Cold Spring Harb. Protoc.* **2009**: Pdb.prot5177.

Collyer, M.L. & Adams, D.C. 2007. Analysis of two-state multivariate phenotypic change in ecological studies. *Ecology* **88**: 683–692.

Collyer, M.L., Sekora, D.J. & Adams, D.C. 2015. A method for analysis of phenotypic change for phenotypes described by high-dimensional data. *Heredity* **115**: 357–365.

Colosimo, P.F., Hosemann, K.E., Balabhadra, S., Villarreal, G., Dickson, M., Grimwood, J., *et al.* 2005. Widespread parallel evolution in sticklebacks by repeated fixation of Ectodysplasin alleles. *Science* **307**: 1928–1933.

Conte, G.L., Arnegard, M.E., Peichel, C.L. & Schluter, D. 2012. The probability of genetic parallelism and convergence in natural populations. *Proc. R. Soc. B* **279**: 5039–5047.

Danecek, P., Auton, A., Abecasis, G., Albers, C.A., Banks, E., DePristo, M.A., *et al.* 2011. The variant call format and VCFtools. *Bioinformatics* **27**: 2156–2158.

De Lisle, S.P. & Bolnick, D.I. 2020. A multivariate view of parallel evolution. *Evolution* evo.14035.

Deagle, B.E., Jones, F.C., Chan, Y.F., Absher, D.M., Kingsley, D.M. & Reimchen, T.E. 2012. Population genomics of parallel phenotypic evolution in stickleback across stream–lake ecological transitions. *Proc. R. Soc. B* **279**: 1277–1286.

Dean, L.L., Magalhaes, I.S., Foote, A., D'Agostino, D., McGowan, S. & MacColl, A.D.C. 2019. Admixture between ancient lineages, selection, and the formation of sympatric stickleback species-pairs. *Mol. Biol. Evol.* **36**: 2481–2497.

Elmer, K.R., Fan, S., Kusche, H., Luise Spreitzer, M., Kautt, A.F., Franchini, P., *et al.* 2014. Parallel evolution of Nicaraguan crater lake cichlid fishes via non-parallel routes. *Nat. Commun.* **5**: 5168.

Elmer, K.R., Kusche, H., Lehtonen, T.K. & Meyer, A. 2010. Local variation and parallel evolution: morphological and genetic diversity across a species complex of neotropical crater lake cichlid fishes. *Philos. Trans. R. Soc. B* **365**: 1763–1782.

Elmer, K.R. & Meyer, A. 2011. Adaptation in the age of ecological genomics: insights from parallelism and convergence. *Trends Ecol. Evol.* **26**: 298–306.

Faria, R., Johannesson, K., Butlin, R.K. & Westram, A.M. 2019. Evolving inversions. *Trends Ecol. Evol.* **34**: 239–248.

Foll, M. & Gaggiotti, O. 2008. A genome-scan method to identify selected loci appropriate for both dominant and codominant markers: A Bayesian perspective. *Genetics* **180**: 977–993.

Foster, S.A., McKinnon, G.E., Steane, D.A., Potts, B.M. & Vaillancourt, R.E. 2007. Parallel evolution of dwarf ecotypes in the forest tree *Eucalyptus globulus*. *New Phytol.* **175**: 370–380.

Fox, J., Friendly, M. & Monette, G. 2018. *heplots: Visualizing Tests in Multivariate Linear Models*. R package version 1.3-5. https://CRAN.R-project.org/package=heplots.

Fraïsse, C. & Welch, J.J. 2019. The distribution of epistasis on simple fitness landscapes. *Biol. Lett.* **15**: 20180881.

Garrison, E. 2016. *Vcflib, a simple C++ library for parsing and manipulating VCF files.* https://github.com/vcflib/vcflib.

Garrison, E. & Marth, G. 2012. Haplotype-based variant detection from short-read sequencing. arXiv. arXiv:1207.3907v2 [q-bio.GN].

Gompel, N. & Prud'homme, B. 2009. The causes of repeated genetic evolution. *Dev. Biol.* **332**: 36–47.

González, J. & Petrov, D.A. 2009. The adaptive role of transposable elements in the Drosophila genome. *Gene* **448**: 124–133.

Haas, O. & Simpson, G.G. 1946. Analysis of some phylogenetic terms, with attempts at redefinition. *Proc. Am. Philos. Soc.* **90**: 319–349.

Harper, R.M., Stowe-Evans, E.L., Luesse, D.R., Muto, H., Tatematsu, K., Watahiki, M.K., *et al.* 2000. The *NPH4* locus encodes the auxin response factor ARF7, a conditional regulator of differential growth in aerial *Arabidopsis* tissue. *Plant Cell* **12**: 757–770.

Hartigan, J.A. & Wong, M.A. 1979. A K-Means clustering algorithm. *Appl. Stat.* **28**: 100.

Hendry, A.P., Kaeuffer, R., Crispo, E., Peichel, C.L. & Bolnick, D.I. 2013. Evolutionary inferences from the analysis of exchangeability. *Evolution* **67**: 3429–3441.

Hoban, S., Kelley, J.L., Lotterhos, K.E., Antolin, M.F., Bradburd, G., Lowry, D.B., *et al.* 2016. Finding the genomic basis of local adaptation: pitfalls, practical solutions, and future directions. *Am. Nat.* **188**: 379–397.

Huang, D.W., Sherman, B.T. & Lempicki, R.A. 2009a. Bioinformatics enrichment tools: paths toward the comprehensive functional analysis of large gene lists. *Nucleic Acids Res.* **37**: 1–13.

Huang, D.W., Sherman, B.T. & Lempicki, R.A. 2009b. Systematic and integrative analysis of large gene lists using DAVID bioinformatics resources. *Nat. Protoc.* **4**: 44–57.

Jacobs, A., Carruthers, M., Yurchenko, A., Gordeeva, N.V., Alekseyev, S.S., Hooker, O., *et al.* 2020. Parallelism in eco-morphology and gene expression despite variable evolutionary and genomic backgrounds in a Holarctic fish. *PLoS Genet.* **16**: e1008658.

James, M.E., Arenas-Castro, H., Groh, J.S., Engelstädter, J. & Ortiz-Barrientos, D. 2020. Highly replicated evolution of parapatric ecotypes. BioRxiv [Preprint]. https://doi.org/10.1101/2020.02.05.936401.

Johannesson, K., Johannesson, B. & Rolán-Alvarez, E. 1993. Morphological differentiation and genetic cohesiveness over a microenvironmental gradient in the marine snail *Littorina saxatilis*. *Evolution* **47**: 1770–1787.

Johannesson, K., Panova, M., Kemppainen, P., André, C., Rolán-Alvarez, E. & Butlin, R.K. 2010. Repeated evolution of reproductive isolation in a marine snail: unveiling mechanisms of speciation. *Philos. Trans. R. Soc. B* **365**: 1735–1747.

Jones, F.C., Chan, Y.F., Russell, P., Mauceli, E., Johnson, J., Swofford, R., *et al.* 2012. The genomic basis of adaptive evolution in threespine sticklebacks. *Nature* **484**: 55–61.

Kautt, A.F., Elmer, K.R. & Meyer, A. 2012. Genomic signatures of divergent selection and speciation patterns in a 'natural experiment', the young parallel radiations of Nicaraguan crater lake cichlid fishes. *Mol. Ecol.* **21**: 4770–4786.

Kirkpatrick, M. & Barton, N. 2006. Chromosome inversions, local adaptation and speciation. *Genetics* **173**: 419–434.

Klepikova, A.V., Kasianov, A.S., Gerasimov, E.S., Logacheva, M.D. & Penin, A.A. 2016. A high resolution map of the *Arabidopsis thaliana* developmental transcriptome based on RNA-seq profiling. *Plant J.* **88**: 1058–1070.

Knotek, A., Konečná, V., Wos, G., Požárová, D., Šrámková, G., Bohutínská, M., *et al.* 2020. Parallel alpine differentiation in *Arabidopsis arenosa*. BioRxiv [Preprint]. https://doi.org/10.1101/2020.02.13.948158.

Konečná, V., Nowak, M.D. & Kolář, F. 2019. Parallel colonization of subalpine habitats in the central European mountains by *Primula elatior*. *Sci. Rep.* **9**: 3294.

Kowalko, J.E., Rohner, N., Linden, T.A., Rompani, S.B., Warren, W.C., Borowsky, R., *et al.* 2013. Convergence in feeding posture occurs through different genetic loci in independently evolved cave populations of *Astyanax mexicanus*. *PNAS* **110**: 16933–16938.

Kusche, H., Elmer, K.R. & Meyer, A. 2015. Sympatric ecological divergence associated with a color polymorphism. *BMC Biol.* **13**: 82.

Lamichhaney, S., Fuentes-Pardo, A.P., Rafati, N., Ryman, N., McCracken, G.R., Bourne, C., *et al.* 2017. Parallel adaptive evolution of geographically distant herring populations on both sides of the North Atlantic Ocean. *PNAS* **114**: E3452–E3461.

Langerhans, R.B. 2018. Predictability and parallelism of multitrait adaptation. *J. Hered.* **109**: 59–70.

Langerhans, R.B. & DeWitt, T.J. 2004. Shared and unique features of evolutionary diversification. *Am. Nat.* **164**: 335–349.

Laporte, M., Rogers, S.M., Dion-Côté, A.-M., Normandeau, E., Gagnaire, P.-A., Dalziel, A.C., *et al.* 2015. RAD-QTL mapping reveals both genome-level parallelism and different genetic architecture underlying the evolution of body shape in lake whitefish (*Coregonus clupeaformis*) species pairs. *G3* **5**: 1481–1491.

Lee, K.M. & Coop, G. 2017. Distinguishing among modes of convergent adaptation using population genomic data. *Genetics* **207**: 1591–1619.

Lee, K.M. & Coop, G. 2019. Population genomics perspectives on convergent adaptation. *Philos. Trans. R. Soc. B* **374**: 20180236.

Lenormand, T., Chevin, L.M. & Bataillon, T. 2016. Parallel evolution: what does it (not) tell us and why is it (still) interesting? In: *Chance in Evolution*. Chicago, USA: University Chicago Press.

Lenormand, T., Roze, D. & Rousset, F. 2009. Stochasticity in evolution. *Trends Ecol. Evol.* **24**: 157–165.

Li, H. 2013. Aligning sequence reads, clone sequences and assembly contigs with BWA-MEM. arXiv:1303.3997 [q-bio.GN].

Li, H. 2018. Minimap2: pairwise alignment for nucleotide sequences. *Bioinformatics* **34**: 3094–3100.

Li, H. & Durbin, R. 2009. Fast and accurate short read alignment with Burrows-Wheeler transform. *Bioinformatics* **25**: 1754–1760.

Lim, M.C.W., Witt, C.C., Graham, C.H. & Dávalos, L.M. 2019. Parallel molecular evolution in pathways, genes, and sites in high-elevation hummingbirds revealed by comparative transcriptomics. *Genome Biol. Evol.* **11**: 1573–1585.

Liu, H. 2014. Developing genomic resources for an emerging ecological model species *Senecio lautus*. PhD Thesis. The University of Queensland. doi: https://doi.org/10.14264/uql.2015.456.

Losos, J.B. 2011. Convergence, adaptation, and constraint. *Evolution* **65**: 1827–1840.

Lowry, D.B., Hoban, S., Kelley, J.L., Lotterhos, K.E., Reed, L.K., Antolin, M.F., *et al.* 2017. Breaking RAD: an evaluation of the utility of restriction site-associated DNA sequencing for genome scans of adaptation. *Mol. Ecol. Resour.* **17**: 142–152.

Lowry, D.B. & Willis, J.H. 2010. A widespread chromosomal inversion polymorphism contributes to a major life-history transition, local adaptation, and reproductive isolation. *PLoS Biol.* **8**: e1000500.

MacPherson, A. & Nuismer, S.L. 2017. The probability of parallel genetic evolution from standing genetic variation. *J. Evol. Biol.* **30**: 326–337.

Mantel, N. 1967. The detection of disease clustering and a generalized regression approach. *Cancer Res.* **27**: 209–220.

Marques, D.A., Lucek, K., Sousa, V.C., Excoffier, L. & Seehausen, O. 2019. Admixture between old lineages facilitated contemporary ecological speciation in Lake Constance stickleback. *Nat. Commun.* **10**: 4240.

McGuigan, K. 2006. Studying phenotypic evolution using multivariate quantitative genetics. *Mol. Ecol.* **15**: 883–896.

McGuigan, K., Chenoweth, S.F. & Blows, M.W. 2005. Phenotypic divergence along lines of genetic variance. *Am. Nat.* **165**: 32–43.

McKinney, G.J., Larson, W.A., Seeb, L.W. & Seeb, J.E. 2017. RADseq provides unprecedented insights into molecular ecology and evolutionary genetics: comment on Breaking RAD by Lowry *et al*. (2016). *Mol. Ecol. Resour.* **17**: 356–361.

Melo, M.C., Grealy, A., Brittain, B., Walter, G.M. & Ortiz-Barrientos, D. 2014. Strong extrinsic reproductive isolation between parapatric populations of an Australian groundsel. *New Phytol.* **203**: 323–334.

Melo, M.C., James, M.E., Roda, F., Bernal-Franco, D., Wilkinson, M.J., Liu, H., *et al.* 2019. Evidence for mutation-order speciation in an Australian wildflower. BioRxiv [Preprint]. doi: https://doi.org/10.1101/692673.

Murren, C.J. 2012. The integrated phenotype. *Integr. Comp. Biol.* **52**: 64–76.

Nelson, T.C., Monnahan, P.J., McIntosh, M.K., Anderson, K., MacArthur-Waltz, E., Finseth, F.R., *et al.* 2019. Extreme copy number variation at a tRNA ligase gene affecting phenology and fitness in yellow monkeyflowers. *Mol. Ecol.* **28**: 1460–1475.

Nosil, P., Crespi, B.J. & Sandoval, C.P. 2002. Host-plant adaptation drives the parallel evolution of reproductive isolation. *Nature* **417**: 440–443.

Oke, K.B., Bukhari, M., Kaeuffer, R., Rolshausen, G., Räsänen, K., Bolnick, D.I., *et al.* 2016. Does plasticity enhance or dampen phenotypic parallelism? A test with three lake-stream stickleback pairs. *J. Evol. Biol.* **29**: 126–143.

Oke, K.B., Rolshausen, G., LeBlond, C. & Hendry, A.P. 2017. How parallel is parallel evolution? A comparative analysis in fishes. *Am. Nat.* **190**: 1–16.

Ord, T.J. & Summers, T.C. 2015. Repeated evolution and the impact of evolutionary history on adaptation. *BMC Evol. Biol.* **15**: 137.

Ortiz-Barrientos, D. & James, M.E. 2017. Evolution of recombination rates and the genomic landscape of speciation. *J. Evol. Biol.* **30**: 1519–1521.

Ostevik, K.L., Moyers, B.T., Owens, G.L. & Rieseberg, L.H. 2012. Parallel ecological speciation in plants? *Int. J. Ecol.* **2012**: 1–17.

Owttrim, G.W. 2006. RNA helicases and abiotic stress. *Nucleic Acids Res.* **34**: 3220–3230.

Paccard, A., Hanson, D., Stuart, Y.E., von Hippel, F.A., Kalbe, M., Klepaker, T., *et al.* 2019. Repeatability of adaptive radiation depends on spatial scale: Regional versus global replicates of stickleback in lake versus stream habitats. *J. Hered.* esz056.

Pérez-Pereira, N., Quesada, H. & Caballero, A. 2017. Can parallel ecological speciation be detected with phylogenetic analyses? *Mol. Phylogenet. Evol.* **116**: 149–156.

Perreault-Payette, A., Muir, A.M., Goetz, F., Perrier, C., Normandeau, E., Sirois, P., *et al.* 2017. Investigating the extent of parallelism in morphological and genomic divergence among lake trout ecotypes in Lake Superior. *Mol. Ecol.* **26**: 1477–1497.

Pilakouta, N., Humble, J.L., Hill, I.D.C., Kristjánsson, B.K., Skúlason, S., Killen, S.S., *et al.* 2019. Testing the predictability of morphological evolution in naturally warmed stickleback populations. BioRxiv [Preprint]. doi: https://dx.doi.org/10.1101/609933.

Poland, J.A., Brown, P.J., Sorrells, M.E. & Jannink, J.L. 2012. Development of high-density genetic maps for barley and wheat using a novel two-enzyme Genotyping-by-Sequencing approach. *PLoS ONE* **7**: e32253.

Pruitt, K.D. 2004. NCBI Reference Sequence (RefSeq): a curated non-redundant sequence database of genomes, transcripts and proteins. *Nucleic Acids Res.* **33**: D501–D504.

Purcell, S., Neale, B., Todd-Brown, K., Thomas, L., Ferreira, M.A.R., Bender, D., *et al.* 2007. PLINK: A tool set for whole-genome association and population-based linkage analyses. *Am. J. Hum. Genet.* **81**: 559–575.

Puritz, J.B., Hollenbeck, C.M. & Gold, J.R. 2014. *dDocent*: a RADseq, variant-calling pipeline designed for population genomics of non-model organisms. *PeerJ* **2**: e431.

Quesada, H., Posada, D., Caballero, A., Morán, P. & Rolán-Alvarez, E. 2007. Phylogenetic evidence for multiple sympatric ecological diversification in a marine snail. *Evolution* **61**: 1600–1612.

R Core Team. 2017. *R: A language and environment for statistical computing.* R Foundation for Statistical Computing. Vienna, Austria. https://www.R-project.org/.

Ralph, P. & Coop, G. 2010. Parallel adaptation: One or many waves of advance of an advantageous allele? *Genetics* **186**: 647–668.

Ravinet, M., Prodöhl, P.A. & Harrod, C. 2013. Parallel and nonparallel ecological, morphological and genetic divergence in lake-stream stickleback from a single catchment. *J. Evol. Biol.* **26**: 186–204.

Reeve, J., Ortiz-Barrientos, D. & Engelstädter, J. 2016. The evolution of recombination rates in finite populations during ecological speciation. *Proc. R. Soc. B* **283**: 20161243.

Richards, T.J. & Ortiz-Barrientos, D. 2016. Immigrant inviability produces a strong barrier to gene flow between parapatric ecotypes of *Senecio lautus*. *Evolution* **70**: 1239–1248.

Richards, T.J., Walter, G.M., McGuigan, K. & Ortiz-Barrientos, D. 2016. Divergent natural selection drives the evolution of reproductive isolation in an Australian wildflower. *Evolution* **70**: 1993–2003.

Rivas, M.J., Saura, M., Pérez-Figueroa, A., Panova, M., Johansson, T., André, C., *et al.* 2018. Population genomics of parallel evolution in gene expression and gene sequence during ecological adaptation. *Sci. Rep.* **8**: 16147.

Roda, F., Ambrose, L., Walter, G.M., Liu, H.L., Schaul, A., Lowe, A., *et al.* 2013a. Genomic evidence for the parallel evolution of coastal forms in the *Senecio lautus* complex. *Mol Ecol* **22**: 2941–2952.

Roda, F., Liu, H., Wilkinson, M.J., Walter, G.M., James, M.E., Bernal, D.M., *et al.* 2013b. Convergence and divergence during the adaptation to similar environments by an Australian groundsel. *Evolution* **67**: 2515–2529.

Rosenblum, E.B., Parent, C.E. & Brandt, E.E. 2014. The molecular basis of phenotypic convergence. *Annu. Rev. Ecol. Evol. Syst.* **45**: 203–226.

Samuk, K., Manzano-Winkler, B., Ritz, K.R. & Noor, M.A.F. 2020. Natural selection shapes variation in genome-wide recombination rate in *Drosophila pseudoobscura*. *Curr. Biol.* **30**: 1517-1528.e6.

Schluter, D. 2000. *The ecology of adaptive radiation*. Oxford, UK: Oxford University Press.

Schluter, D. & Nagel, L.M. 1995. Parallel speciation by natural selection. *Am. Nat.* **146**: 292–301.

Schmieder, R., Lim, Y.W., Rohwer, F. & Edwards, R. 2010. TagCleaner: Identification and removal of tag sequences from genomic and metagenomic datasets. *BMC Bioinformatics* **11**: 341.

Schneider, C.A., Rasband, W.S. & Eliceiri, K.W. 2012. NIH Image to ImageJ: 25 years of image analysis. *Nat. Methods* **9**: 671–675.

Schrader, L. & Schmitz, J. 2019. The impact of transposable elements in adaptive evolution. *Mol. Ecol.* **28**: 1537–1549.

Schrider, D.R., Hahn, M.W. & Begun, D.J. 2016. Parallel evolution of copy-number variation across continents in *Drosophila melanogaster*. *Mol. Biol. Evol.* **33**: 1308–1316.

Smith, S.D. & Rausher, M.D. 2011. Gene loss and parallel evolution contribute to species difference in flower color. *Mol. Biol. Evol.* **28**: 2799–2810.

Soria-Carrasco, V., Gompert, Z., Comeault, A.A., Farkas, T.E., Parchman, T.L., Johnston, J.S., *et al.* 2014. Stick insect genomes reveal natural selection's role in parallel speciation. *Science* **344**: 738–742.

Speed, M.P. & Arbuckle, K. 2017. Quantification provides a conceptual basis for convergent evolution. *Biol. Rev.* **92**: 815–829.

Staswick, P.E., Serban, B., Rowe, M., Tiryaki, I., Maldonado, M.T., Maldonado, M.C., *et al.* 2005. Characterization of an *Arabidopsis* enzyme family that conjugates amino acids to indole-3-acetic acid. *Plant Cell* **17**: 616–627.

Stayton, C.T. 2008. Is convergence surprising? An examination of the frequency of convergence in simulated datasets. *J. Theor. Biol.* **252**: 1–14.

Stern, D.L. 2013. The genetic causes of convergent evolution. *Nat. Rev. Genet.* **14**: 751–764.

Stern, D.L. & Orgogozo, V. 2009. Is genetic evolution predictable? *Science* **323**: 746–751.

Stoltzfus, A. & McCandlish, D.M. 2017. Mutational biases influence parallel adaptation. *Mol. Biol. Evol.* **34**: 2163–2172.

Strohm, A.K., Baldwin, K.L. & Masson, P.H. 2012. Multiple roles for membrane-associated protein trafficking and signaling in gravitropism. *Front. Plant Sci.* **3**.

Stuart, Y.E. 2019. Divergent uses of "parallel evolution" during the history of *The American Naturalist*. *Am. Nat.* **193**: 11–19.

Stuart, Y.E., Veen, T., Weber, J.N., Hanson, D., Ravinet, M., Lohman, B.K., *et al.* 2017. Contrasting effects of environment and genetics generate a continuum of parallel evolution. *Nat. Ecol. Evol.* **1**: 0158.

Tenaillon, O., Rodriguez-Verdugo, A., Gaut, R.L., McDonald, P., Bennett, A.F., Long, A.D., *et al.* 2012. The molecular diversity of adaptive convergence. *Science* **335**: 457–461.

Thompson, K.A., Osmond, M.M. & Schluter, D. 2019. Parallel genetic evolution and speciation from standing variation. *Evol. Lett.* **3**: 129–141.

Tiffin, P. & Ross-Ibarra, J. 2014. Advances and limits of using population genetics to understand local adaptation. *Trends Ecol. Evol.* **29**: 673–680.

Trucchi, E., Frajman, B., Haverkamp, T.H.A., Schönswetter, P. & Paun, O. 2017. Genomic analyses suggest parallel ecological divergence in *Heliosperma pusillum* (Caryophyllaceae). *New Phytol.* **216**: 267–278.

VanWallendael, A., Soltani, A., Emery, N.C., Peixoto, M.M., Olsen, J. & Lowry, D.B. 2019. A molecular view of plant local adaptation: Incorporating stress-response networks. *Annu. Rev. Plant Biol.* **70**: 559–583.

Verta, J.P. & Jones, F.C. 2019. Predominance of cis-regulatory changes in parallel expression divergence of sticklebacks. *eLife* **8**: e43785.

Walter, G.M., Aguirre, J.D., Blows, M.W. & Ortiz-Barrientos, D. 2018a. Evolution of genetic variance during adaptive radiation. *Am. Nat.* **191**: E108–E128.

Walter, G.M., Wilkinson, M.J., Aguirre, J.D., Blows, M.W. & Ortiz-Barrientos, D. 2018b. Environmentally induced development costs underlie fitness tradeoffs. *Ecology* **99**: 1391–1401.

Walter, G.M., Wilkinson, M.J., James, M.E., Richards, T.J., Aguirre, J.D. & Ortiz-Barrientos, D. 2016. Diversification across a heterogeneous landscape. *Evolution* **70**: 1979–1992.

Weir, B.S. & Cockerham, C.C. 1984. Estimating F-Statistics for the analysis of population structure. *Evolution* **38**: 1358.

Wellenreuther, M., Mérot, C., Berdan, E. & Bernatchez, L. 2019. Going beyond SNPs: The role of structural genomic variants in adaptive evolution and species diversification. *Mol. Ecol.* **28**: 1203–1209.

Wilkinson, M.J., Roda, F., Walter, G.M., James, M.E., Nipper, R., Walsh, J., *et al.* 2020. Divergence in hormone signaling drives local adaptation and intrinsic reproductive isolation. BioRxiv [Preprint]. https://doi.org/10.1101/845354.

Wood, T.E., Burke, J.M. & Rieseberg, L.H. 2005. Parallel genotypic adaptation: when evolution repeats itself. *Genetica* **123**: 157–170.

Yeaman, S. 2015. Local adaptation by alleles of small effect. *Am. Nat.* **186**: S74–S89.

Figures

Figure 1. A framework to measure phenotypic and genotypic parallel evolution

Parallel evolution can be broken down into two components: the phenotype and the genotype. These two components can be measured in the broad-sense (the overall differences between ecotypes), and the narrow-sense (the specific similarities between replicate pairs). Broad-sense phenotypic parallelism can be measured at the level of the ecotype and trait, whereas narrow-sense phenotypic parallelism is measured at the level of the pair. Genotypic parallelism can be measured at different biological levels of organization in both the broad- and narrow-sense scales: the nucleotide site, gene, and biological function.

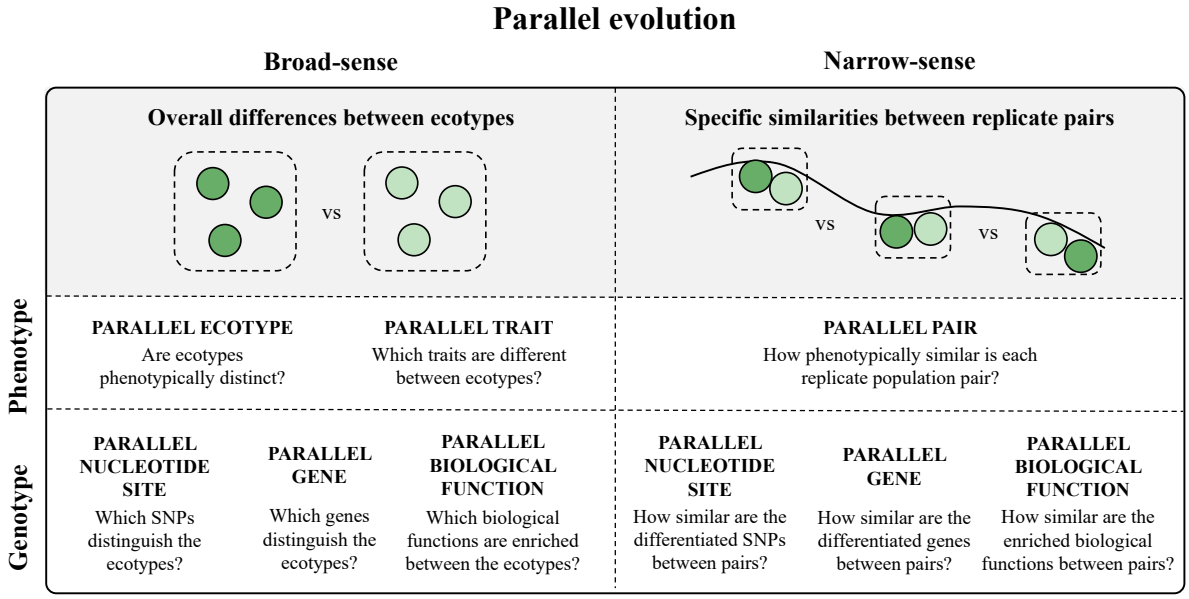

Figure 2. Broad-sense phenotypic parallelism in *S. lautus*: parallel ecotype

(A) Sampling locations of the 22 Dune (orange) and Headland (green) *Senecio lautus* populations along the coast of Australia. **(B)** Maximum likelihood phylogeny of Dune and Headland populations implemented in IQ-TREE. Numbers on each node represent the SH-alRT support (%), followed by the ultrafast bootstrap support (%). Modified with permission from James *et al.*, (2020). The intermediate population (H12A) is not included within this study. **(C)** Partial effect sizes (partial η^2) for the ecotype and the interaction (ecotype × pair) for the trait-by-trait linear models, each dot representing a single trait. The red dot represents Wilk's partial effect size for all traits combined within the MANOVA. Dashed line is a 1:1 ratio, where points above the line represent a larger contribution of broad- to narrow-sense divergence. See Table S4 for details. **(D)** Schematic diagram of Dune and Headland ecotypes based on mean trait values from linear discriminant analysis (LDA) shown in Figure 3C. **(E)** Principal component analysis of Dune and Headland phenotypes (five plant architecture and four leaf traits) across 20 populations. Ecotypes are delimited by 70% probability ellipses.

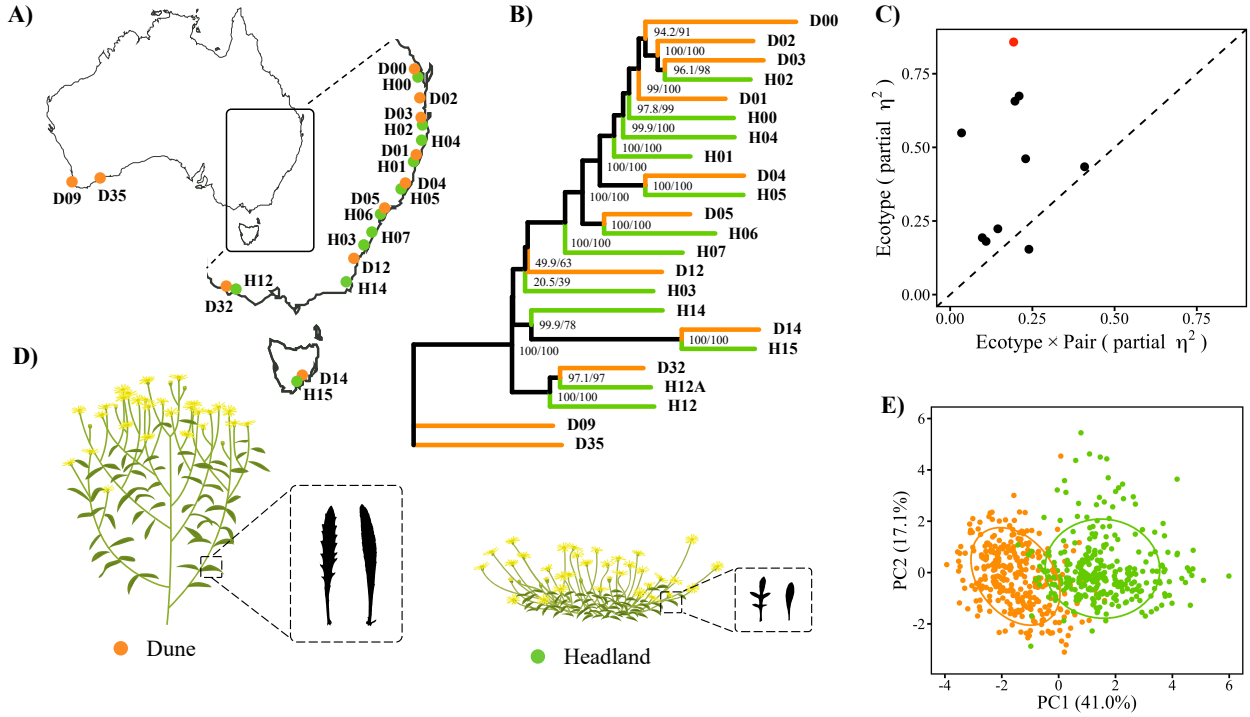

Figure 3. Broad-sense phenotypic parallelism in *S. lautus*: parallel trait

(A) Vote-counting for five plant architecture and four leaf traits across eight replicate pairs. Dots represent the mean trait value for each population (N = 30). Lines connect the Dune (orange) populations to their Headland (green) pair. Dashed lines represent pairs whose Dune-Headland trait value is in the opposite direction from the majority of pairs. Asterisks denote significance (** S-statistic = 8, P = 0.0078; * S-statistic = 7, P = 0.035). **(B)** Frequency distribution of the ecotype R^2 values (proportion of phenotypic variance explained by the ecotype term) for each trait from one-way ANOVAs performed on the population means. **(C)** Linear discriminant analysis of all traits between Dune and Headland ecotypes.

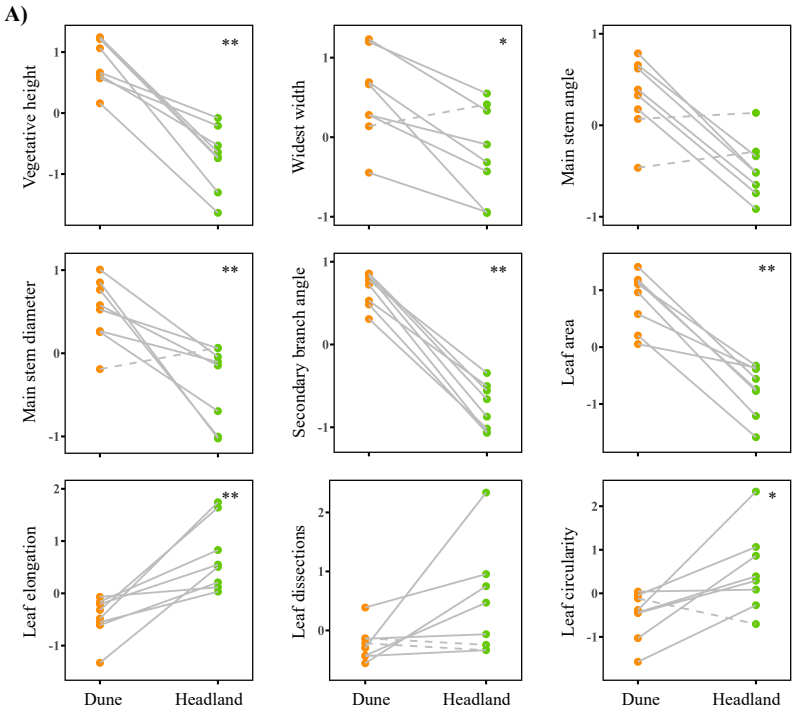

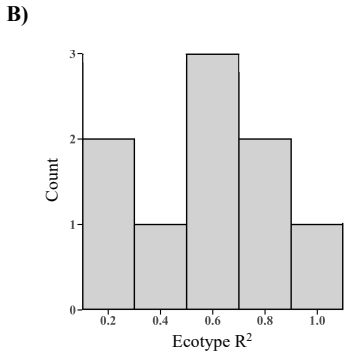

C)

Trait Category	Trait	LDA
Architecture	Vegetative height	**-0.26**
	Widest width	**0.41**
	Main stem angle	-0.15
	Main stem diameter	**-0.36**
	Secondary branch angle	**-0.61**
Leaf	Area	**-0.78**
	Elongation	-0.01
	Dissection	**0.51**
	Circularity	**0.45**

Figure 4. Narrow-sense phenotypic parallelism in *S. lautus*: parallel pair

(A) PC1 and PC2 for five plant architecture and four leaf traits across eight replicate Dune-Headland pairs. Each dot represents the population centroid (multivariate phenotypic mean), ± SE. The Dune (orange) and Headland (green) populations of a replicate pair are connected with a line. **(B)** Frequency distribution of the 28 pairwise phenotypic divergences (ΔL) between Dune-Headland replicate pairs (Table S6). **(C)** Frequency distribution of the 28 pairwise contribution of traits (θ) between Dune-Headland replicate pairs (Table S9).

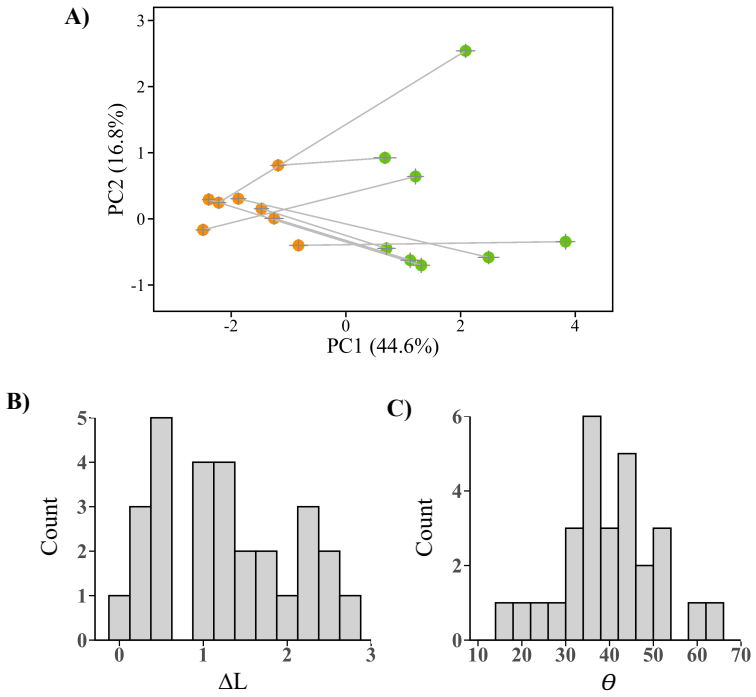

Figure 5. Relative contributions of broad- and narrow-sense genotypic parallelism in *S. lautus*

Partial effect sizes (partial η^2) for the ecotype and the interaction (ecotype × pair) for the linear models for nucleotide sites **(A)** genes **(B)**. Each dot represents either a single SNP **(A)** or gene **(B)**. Dashed line is a 1:1 ratio, where points above the line represent a larger contribution of broad- to narrow-sense parallelism. The red dots denote broad-sense outlier SNPs **(A)** and genes **(B)**. Partial effect size frequency distributions for the nucleotide sites **(C)** and genes **(D)**. Values above zero represent a larger contribution of broad- to narrow-sense parallelism.

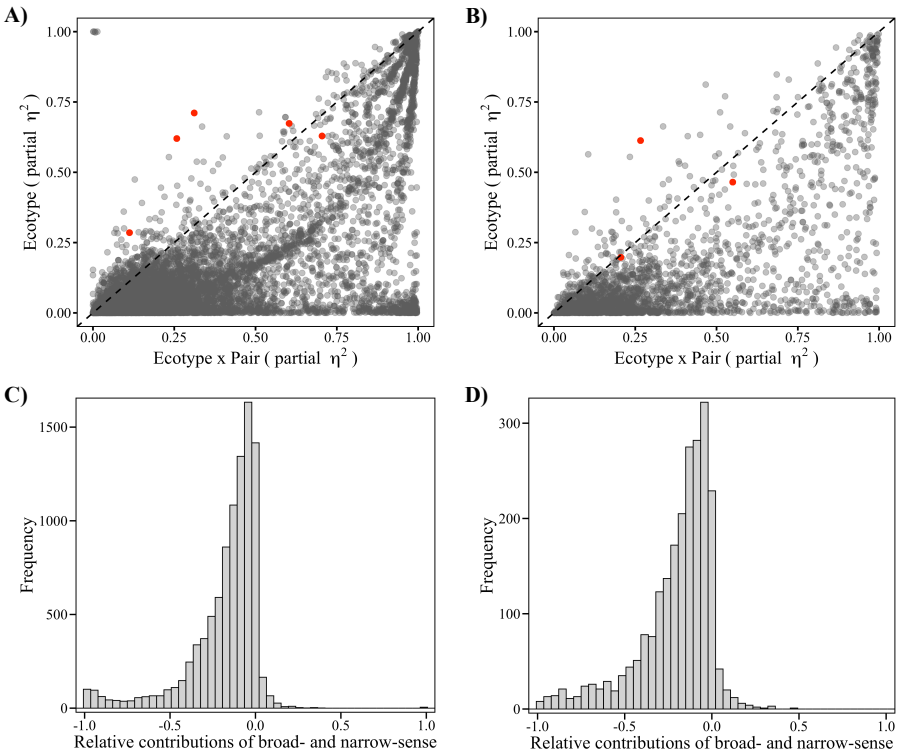

Figure 6. Broad- and narrow-sense genotypic parallelism in *S. lautus*

(A) Broad-sense parallel nucleotide sites showing high differentiation between the Dune-Headland ecotypes as well as concordant allele frequency changes across replicate pairs. Dots represent the allele frequency value (of the reference allele) for each population. Lines connect the Dune (orange) populations to their Headland (green) pair. Dashed lines represent pairs whose Dune-Headland change in allele frequency is in the opposite direction from the majority of pairs. Δ*p* denotes the overall change in allele frequency between the ecotypes. *G* denotes SNPs that occur within genic regions. **(B)** Proportion of outlier nucleotide sites, outlier genes, and enriched biological functions shared across the nine replicate pairs. **(C)** Enriched biological functions shared across five or more replicate population pairs.

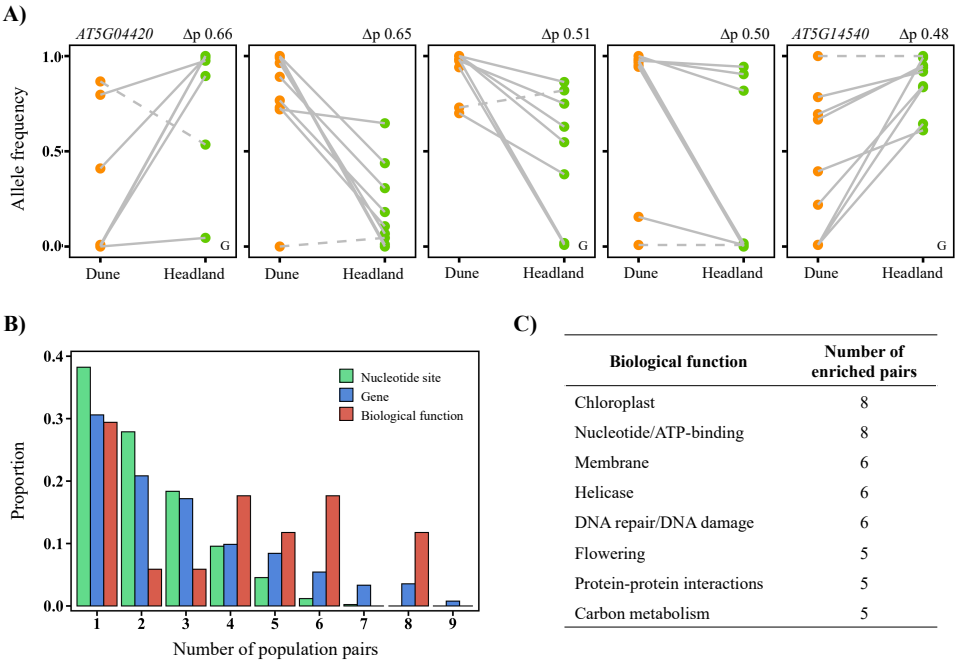

C)

Biological function	Number of enriched pairs
Chloroplast	8
Nucleotide/ATP-binding	8
Membrane	6
Helicase	6
DNA repair/DNA damage	6
Flowering	5
Protein-protein interactions	5
Carbon metabolism	5

Supplementary Tables and Figures

Table S1. *Senecio lautus* sampling locations in this study

Sampling locations of the 22 *Senecio lautus* Dune and Headland populations. Coordinates represent the mid-point of each population. N genetics and N phenotype represent the sample sizes used for the genotypic and phenotypic analysis respectively. Note: N genetics corresponds to the final number of individuals after removing those with low coverage. Pairs in bold are sister-taxa within the phylogeny.

Clade	Population code	Location	Ecotype	Pair	Coordinates	N genetics	N phenotype
Eastern	D00	QLD: Stradbroke Island	Dune	D00-H00	S27° 31.153' E153° 30.189'	62	30
Eastern	H00	QLD: Stradbroke Island	Headland	D00-H00	S27° 26.140' E153° 32.749'	63	30
Eastern	D02	QLD: Southport	Dune	D02-H04	S27° 56.846' E153° 25.736'	62	30
Eastern	H04	NSW: Byron Bay	Headland	D02-H04	S28° 38.060' E153° 38.268'	62	30
Eastern	D03	NSW: Cabarita	Dune	**D03-H02**	S28° 19.794' E153° 34.264'	61	30
Eastern	H02	NSW: Cabarita	Headland	**D03-H02**	S28° 21.013' E153° 34.676'	61	30
Eastern	D01	QLD: Lennox Head	Dune	D01-H01	S28° 46.858' E153° 35.655'	60	30
Eastern	H01	QLD: Lennox Head	Headland	D01-H01	S28° 48.813' E153° 36.313'	58	30
Eastern	D04	NSW: Coffs Harbour	Dune	**D04-H05**	S30° 18.946' E153° 08.142'	62	30
Eastern	H05	NSW: Coffs Harbour	Headland	**D04-H05**	S30° 18.741' E153° 08.676'	62	30
Eastern	D05	NSW: South West Rocks	Dune	**D05-H06**	S30° 53.027' E153° 04.037'	62	30
Eastern	H06	NSW: South West Rocks	Headland	**D05-H06**	S30° 52.710' E153° 04.549'	62	30
Southern	H07	NSW: Port Macquarie	Headland	-	S31° 28.526' E152° 56.219	-	30
Southern	H03	NSW: Kiama	Headland	-	S34° 40.301' E150° 51.704'	-	29
Southern	D12	NSW: Bermagui	Dune	D12-H14	S36° 28.346' E150° 03.581'	62	31
Southern	H14	NSW: Green Cape	Headland	D12-H14	S37° 15.748' E150° 02.991'	62	30
Southern	D32	VIC: Cape Bridgewater	Dune	**D32-H12**	S38° 19.631' E141° 23.772'	62	30
Southern	H12	VIC: Cape Bridgewater	Headland	**D32-H12**	S38° 22.728' E141° 22.018'	63	30
Southern	D14	TAS: Port Arthur	Dune	**D14-H15**	S43° 10.550' E147° 51.267'	12	-
Southern	H15	TAS: Port Arthur	Headland	**D14-H15**	S43° 11.240' E147° 50.672'	11	-
Western	D35	WA: Isthmus Hill	Dune	-	S35° 05.885' E117° 59.182'	-	34
Western	D09	WA: Leeuwin-Naturaliste National Park	Dune	-	S33° 46.239' E114° 59.541'	-	31

Table S2. *Senecio lautus* phenotypic traits

Traits with asterisks were removed from the analysis due to high correlations (> 0.8).

Trait category	Trait	Description
Plant architecture	Vegetative height	Base of plant to highest vegetative leaf (not including flowers)
	Widest width	Widest with of plant between vegetative leaves
	Narrowest width*	Narrowest width of plant between vegetative leaves
	Main stem angle	Angle of main stem measured from base of soil
	Main stem diameter	Diameter of main stem measured 1cm above soil
	Secondary branch angle	Average angle of secondary branches
Leaf	Area	Leaf area
	Perimeter*	Leaf perimeter
	Width*	Leaf width
	Height*	Leaf height
	Elongation	Length to width ratio
	Compactness*	Squared perimeter to area ratio
	Dissection	Perimeter to length ratio
	Circularity	4π (area/perimeter^2)

Table S3. Demographic and environmental data for *S. lautus* population pairs

Rates of gene flow (2N*m*, forward in time) and divergence times were calculated in *fastsimcoal2* (see James *et al.*, (2020) for details). 2N*m* (D -> H): gene flow since secondary contact from the Dune to the Headland. 2N*m* (H -> D): gene flow since secondary contact from the Headland to the Dune. 2N*m* (ABS): absolute gene flow since secondary contact. See (Roda *et al.*, 2013b) for details of the environmental distances.

Pair	2Nm (D -> H)	2Nm (H -> D)	2Nm (ABS)	Divergence time (years)	Environmental distance
D00-H00	0.2176	0.2830	0.065424	71945	3.23
D02-H04	0.2697	0.1720	0.097695	82539	NA
D03-H02	0.1590	0.4722	0.313209	44190	10.26
D01-H01	0.6241	0.3671	0.256984	71918	13.68
D04-H05	**1.3942**	**1.5024**	0.108212	30707	6.31
D05-H06	0.4049	0.4325	0.027621	67927	NA
D12-H14	0.2188	0.1787	0.040083	47929	5.14
D32-H12	**5.5694**	**5.2694**	0.300057	38706	NA

Table S4. Trait-by-trait linear models and partial effect sizes

F-values and P-values for the ecotype (Ecotype $F_{1,465}$; Ecotype P-value) and interaction (Ecotype x Pair $F_{7,465}$; Ecotype × Pair P-value) for trait-by-trait linear models (*trait* = *ecotype* + *pair* + *ecotype* × *pair*). Partial effect sizes (partial η^2) for the Ecotype, Pair and Interaction (Ecotype × Pair) for each trait.

Trait Category	Trait	Ecotype $F_{1, 465}$	Ecotype P-value	Ecotype × Pair $F_{7, 465}$	Ecotype × Pair P-value	Ecotype partial η^2	Pair partial η^2	Ecotype × Pair partial η^2
Plant architecture	Vegetative height	962.65	$< 2.2 \times 10^{-16}$ ***	17.63	$< 2.2 \times 10^{-16}$ ***	0.67	0.26	0.21
	Widest width	102.62	$< 2.2 \times 10^{-16}$ ***	8.14	2.3×10^{-9} ***	0.18	0.30	0.11
	Main stem angle	111.35	$< 2.2 \times 10^{-16}$ ***	7.20	3.4×10^{-8} ***	0.19	0.06	0.10
	Main stem diameter	133.75	$< 2.2 \times 10^{-16}$ ***	11.26	3.3×10^{-13} ***	0.22	0.07	0.14
	Secondary branch angle	566.05	$< 2.2 \times 10^{-16}$ ***	2.39	0.02092 *	0.55	0.08	0.03
Leaf	Area	889.52	$< 2.2 \times 10^{-16}$ ***	16.30	$< 2.2 \times 10^{-16}$ ***	0.66	0.26	0.20
	Elongation	398.11	$< 2.2 \times 10^{-16}$ ***	19.79	$< 2.2 \times 10^{-16}$ ***	0.46	0.26	0.23
	Dissection	84.64	$< 2.2 \times 10^{-16}$ ***	20.92	$< 2.2 \times 10^{-16}$ ***	0.15	0.25	0.24
	Circularity	356.68	$< 2.2 \times 10^{-16}$ ***	45.92	$< 2.2 \times 10^{-16}$ ***	0.43	0.46	0.41

Table S5. Summary of parallel phenotypic traits in *S. lautus*

Summary of the three approaches to measure phenotypic parallelism per trait (vote-counting, trait-by-trait linear models, and R^2). 'Yes' denotes a trait was either statistically significant using the vote-counting approach (Vote-counting), had a significant ecotype term in the trait-by-trait linear models (Linear models), or an $R^2 \geq 0.50$ for one-way ANOVAs performed on the population means (Ecotype R^2). See main text for details on each approach. Traits in bold are consistently viewed as parallel across each of the three approaches.

Trait Category	Trait	Vote-counting	Linear models	Ecotype R^2
Plant architecture	**Vegetative height**	Yes	Yes	Yes
	Widest width	Yes	Yes	No
	Main stem angle	No	Yes	Yes
	Main stem diameter	Yes	Yes	Yes
	Secondary branch angle	Yes	Yes	Yes
Leaf	**Area**	Yes	Yes	Yes
	Elongation	Yes	Yes	Yes
	Dissection	No	Yes	No
	Circularity	Yes	Yes	No

Table S6. Pairwise change in lengths (ΔL) for all traits in coastal ecotypes of *S. lautus*

Values below the diagonal represent the change in lengths, above the diagonal are the P-values. Shaded cells donate parallel pairs (P > 0.01, i.e., ΔL ≈ 0°).

	D00-H00	**D01-H01**	**D02-H04**	**D03-H02**	**D04-H05**	**D05-H06**	**D12-H14**	**D32-H12**
D00-H00	-	0.3239	0.0001	0.0001	0.0001	0.4949	0.0001	0.0001
D01-H01	0.27	-	0.0001	0.0001	0.0001	0.0763	0.0001	0.0001
D02-H04	2.45	2.72	-	0.0548	0.0002	0.0001	0.0001	0.5683
D03-H02	1.86	2.13	0.59	-	0.0435	0.0001	0.0367	0.1627
D04-H05	1.27	1.54	1.18	0.59	-	0.0003	0.8839	0.0003
D05-H06	0.20	0.47	2.26	1.66	1.08	-	0.0007	0.0001
D12-H14	1.24	1.51	1.22	0.62	0.04	1.04	-	0.0005
D32-H12	2.29	2.56	0.16	0.43	1.02	2.10	1.05	-

Table S7. Pairwise change in lengths (ΔL) for plant architecture traits in coastal ecotypes of *S. lautus*

Values below the diagonal represent the change in lengths, above the diagonal are the P-values. Shaded cells donate parallel pairs (P > 0.01, i.e., ΔL ≈ 0°).

	D00-H00	**D01-H01**	**D02-H04**	**D03-H02**	**D04-H05**	**D05-H06**	**D12-H14**	**D32-H12**
D00-H00	-	0.1366	0.0001	0.0001	0.0001	0.6428	0.0016	0.0008
D01-H01	0.44	-	0.0001	0.0001	0.0001	0.0394	0.0002	0.0001
D02-H04	1.55	1.99	-	0.0926	0.4009	0.0001	0.0477	0.1153
D03-H02	2.08	2.52	0.53	-	0.0056	0.0001	0.0001	0.0017
D04-H05	1.32	1.76	0.23	0.77	-	0.0001	0.1633	0.3648
D05-H06	0.14	0.58	1.41	1.94	1.18	-	0.0070	0.0032
D12-H14	0.94	1.38	0.61	1.14	0.37	0.80	-	0.6626
D32-H12	1.07	1.52	0.48	1.01	0.24	0.94	0.13	-

Table S8. Pairwise change in lengths (ΔL) for leaf traits in coastal ecotypes of *S. lautus*

Values below the diagonal represent the change in lengths, above the diagonal are the P-values. Shaded cells donate parallel pairs (P > 0.01, i.e., ΔL ≈ 0°).

	D00-H00	**D01-H01**	**D02-H04**	**D03-H02**	**D04-H05**	**D05-H06**	**D12-H14**	**D32-H12**
D00-H00	-	0.9650	0.0001	0.0740	0.0239	0.4917	0.0006	0.0001
D01-H01	0.01	-	0.0001	0.1268	0.0509	0.5771	0.0046	0.0001
D02-H04	1.90	1.89	-	0.0001	0.0001	0.0001	0.0015	0.4492
D03-H02	0.34	0.34	1.56	-	0.6506	0.3263	0.0352	0.0001
D04-H05	0.43	0.42	1.47	0.09	-	0.1646	0.0674	0.0001
D05-H06	0.14	0.13	1.77	0.21	0.30	-	0.0052	0.0001
D12-H14	0.81	0.80	1.10	0.46	0.37	0.67	-	0.0001
D32-H12	2.08	2.07	0.17	1.73	1.64	1.94	1.27	-

Table S9. Pairwise angles (θ) for all traits in coastal ecotypes of *S. lautus*

Values below the diagonal represent the angles (in degrees), above the diagonal are the P-values. Shaded cells donate parallel pairs ($P > 0.01$, i.e., $\theta \approx 0°$).

	D00-H00	**D01-H01**	**D02-H04**	**D03-H02**	**D04-H05**	**D05-H06**	**D12-H14**	**D32-H12**
D00-H00	-	0.0001	0.0001	0.0001	0.0001	0.0001	0.0001	0.0001
D01-H01	43.38	-	0.0001	0.0001	0.0001	0.0001	0.0018	0.0001
D02-H04	43.73	49.83	-	0.0001	0.0001	0.0001	0.0001	0.0001
D03-H02	31.00	50.52	40.33	-	0.0105	0.0001	0.0001	0.0001
D04-H05	26.57	42.70	42.93	14.51	-	0.0001	0.0001	0.0001
D05-H06	61.69	49.81	62.81	39.29	39.30	-	0.0001	0.0001
D12-H14	50.10	35.99	34.81	34.08	35.69	35.34	-	0.0010
D32-H12	50.27	34.82	45.36	33.59	33.74	24.43	20.14	-

Table S10. Pairwise angles (θ) for plant architecture traits in coastal ecotypes of *S. lautus*

Values below the diagonal represent the angles (in degrees), above the diagonal are the P-values. Shaded cells donate parallel pairs (P > 0.01, i.e., θ ≈ 0°).

	D00-H00	**D01-H01**	**D02-H04**	**D03-H02**	**D04-H05**	**D05-H06**	**D12-H14**	**D32-H12**
D00-H00	-	0.0021	0.0025	0.0049	0.0022	0.0003	0.0013	0.0005
D01-H01	49.70	-	0.0001	0.0001	0.0001	0.0005	0.0002	0.0001
D02-H04	26.78	62.07	-	0.2492	0.0270	0.0002	0.0002	0.0161
D03-H02	23.10	60.56	9.27	-	0.0395	0.0001	0.0009	0.0043
D04-H05	27.06	50.46	15.63	13.48	-	0.0198	0.1135	0.5276
D05-H06	43.11	50.21	30.17	30.37	18.95	-	0.0051	0.0835
D12-H14	31.30	44.17	26.61	22.66	13.08	23.40	-	0.1199
D32-H12	33.60	50.15	18.37	19.47	8.49	17.08	14.04	-

Table S11. Pairwise angles (θ) for leaf traits in coastal ecotypes of *S. lautus*

Values below the diagonal represent the angles (in degrees), above the diagonal are the P-values. Shaded cells donate parallel pairs (P > 0.01, i.e., θ ≈ 0°).

	D00-H00	**D01-H01**	**D02-H04**	**D03-H02**	**D04-H05**	**D05-H06**	**D12-H14**	**D32-H12**
D00-H00	-	0.0014	0.0001	0.0001	0.0012	0.0001	0.0001	0.0001
D01-H01	37.73	-	0.0001	0.1043	0.0172	0.0001	0.0531	0.0009
D02-H04	54.25	40.54	-	0.0001	0.0001	0.0001	0.0001	0.0001
D03-H02	31.56	19.33	58.04	-	0.0907	0.0001	0.0002	0.0001
D04-H05	21.88	26.54	60.06	11.42	-	0.0001	0.0001	0.0001
D05-H06	75.54	48.76	82.96	44.26	54.12	-	0.0001	0.0001
D12-H14	63.73	26.53	40.49	42.27	51.98	43.90	-	0.0060
D32-H12	58.83	24.12	56.47	29.60	40.89	26.79	20.31	-

Table S12. Shared outlier nucleotide sites between replicate population pairs from coastal ecotypes of *S. lautus*

Values below the diagonal represent the number of shared outlier nucleotide sites. Values above the diagonal are the P-values of the probability that the common nucleotide sites are shared by chance, calculated from the hypergeometric distribution.

	D00-H00	**D01-H01**	**D02-H04**	**D03-H02**	**D04-H05**	**D05-H06**	**D12-H14**	**D14-H15**	**D32-H12**
D00-H00	-	3.75E-58	7.72E-54	3.98E-37	5.31E-51	8.48E-42	8.13E-50	2.74E-07	1.68E-32
D01-H01	169	-	3.59E-58	9.08E-52	1.14E-62	1.52E-48	1.39E-51	4.07E-05	6.49E-33
D02-H04	189	161	-	1.58E-49	3.52E-32	1.10E-53	1.20E-37	1.80E-03	3.40E-44
D03-H02	178	164	187	-	8.27E-46	1.36E-46	3.76E-44	2.63E-05	6.47E-36
D04-H05	195	174	155	192	-	5.31E-51	3.60E-44	1.07E-05	4.69E-34
D05-H06	165	144	173	176	178	-	2.27E-58	1.15E-11	7.98E-49
D12-H14	226	185	193	222	216	218	-	6.91E-10	7.40E-68
D14-H15	31	21	21	28	28	35	41	-	1.13E-03
D32-H12	207	164	215	220	210	214	311	30	-

Table S13. Shared outlier genes between replicate population pairs from coastal ecotypes of *S. lautus*

Values below the diagonal represent the number of shared outlier genes. Values above the diagonal are the P-values of the probability that the common genes are shared by chance, calculated from the hypergeometric distribution.

	D00-H00	**D01-H01**	**D02-H04**	**D03-H02**	**D04-H05**	**D05-H06**	**D12-H14**	**D14-H15**	**D32-H12**
D00-H00	-	2.10E-40	2.76E-53	1.54E-34	6.83E-33	2.47E-39	9.75E-24	2.05E-05	1.01E-19
D01-H01	123	-	1.13E-52	1.18E-44	5.03E-45	2.07E-35	2.88E-29	7.56E-04	1.79E-22
D02-H04	156	128	-	8.25E-47	2.06E-34	1.26E-42	5.36E-31	3.48E-05	1.15E-34
D03-H02	137	122	142	-	1.11E-34	1.78E-35	2.78E-22	7.95E-05	1.16E-24
D04-H05	141	127	133	136	-	6.85E-34	1.52E-20	2.30E-03	7.76E-20
D05-H06	146	114	140	134	138	-	1.32E-32	1.25E-08	5.61E-24
D12-H14	171	140	168	158	164	179	-	1.50E-03	2.34E-17
D14-H15	32	22	29	29	27	37	40	-	0.10091
D32-H12	168	133	177	166	167	170	231	35	-

Table S14. Shared biological functions between replicate population pairs from coastal ecotypes of *S. lautus*

Summary of the 17 enriched biological functions across the 9 replicate pairs inferred in *DAVID*. P-values represent the EASE score, a modified Fisher Exact P-value. 'NA' denotes the function was not enriched within the pair.

Biological function	D00-H00	D02-H04	D03-H02	D01-H01	D04-H05	D05-H06	D12-H14	D14-H15	D32-H12
Chloroplast	7.25E-04	4.91E-05	1.08E-04	6.63E-03	8.56E-03	3.02E-02	3.57E-10	NA	4.79E-05
Nucleotide/ATP-binding	1.12E-05	3.05E-03	7.00E-07	5.32E-04	7.74E-04	2.33E-02	7.87E-03	NA	3.77E-07
Membrane	8.50E-04	NA	NA	3.55E-05	1.22E-02	2.25E-02	1.67E-03	NA	9.48E-03
Helicase	2.38E-03	NA	7.20E-03	NA	2.69E-02	1.62E-02	8.08E-04	NA	3.90E-02
DNA repair/DNA damage	NA	3.81E-02	4.32E-02	7.01E-04	4.65E-02	NA	1.42E-03	NA	3.31E-02
Flowering	NA	NA	3.36E-04	5.95E-03	NA	3.60E-02	NA	2.79E-02	1.24E-02
Protein-protein interactions	NA	NA	NA	8.00E-03	1.90E-02	2.96E-02	NA	3.38E-02	1.32E-03
Carbon metabolism	2.37E-02	NA	NA	2.35E-02	4.40E-02	NA	NA	5.93E-03	2.14E-02
Zinc finger	2.47E-02	2.25E-02	NA	NA	NA	1.73E-02	2.28E-03	NA	NA
Nucleus	NA	2.59E-02	1.34E-02	NA	NA	NA	4.36E-03	NA	4.44E-03
ATPase dependent activity	NA	NA	4.08E-03	NA	NA	4.02E-03	4.20E-04	3.55E-02	NA
Catalytic activity	NA	NA	1.34E-02	NA	NA	6.62E-03	5.54E-04	NA	NA
Stress response	NA	NA	NA	NA	NA	3.18E-02	9.14E-03	NA	NA
Auxin pathway	NA	NA	NA	NA	NA	1.16E-02	NA	NA	NA
Amino acid transport	NA	NA	NA	NA	NA	NA	NA	NA	4.29E-03
Glycoprotein	1.63E-02	NA	NA	NA	NA	NA	NA	NA	NA
Endoplasmic reticulum	NA	NA	NA	NA	NA	3.80E-02	NA	NA	NA

Table S15. Shared biological functions between replicate population pairs from coastal ecotypes of *S. lautus* using a more stringent approach

Summary of the 5 enriched biological functions across the 9 replicate pairs inferred in *DAVID*. P-values represent the Benjamini-adjusted P-value. 'NA' denotes the function was not enriched within the pair.

Biological function	D00-H00	D02-H04	D03-H02	D01-H01	D04-H05	D05-H06	D12-H14	D14-H15	D32-H12
Nucleotide /ATP-binding	1.22E-03	NA	1.33E-04	NA	NA	NA	4.07E-08	NA	5.22E-05
Chloroplast	NA	6.12E-03	1.34E-02	NA	NA	NA	NA	NA	7.25E-03
Transmembrane helix	NA	NA	NA	6.20E-03	NA	NA	NA	NA	NA
Flowering	NA	NA	1.27E-02	NA	NA	NA	NA	NA	NA
Ligase	NA	NA	NA	NA	NA	NA	2.01E-02	NA	NA

Figure S1. Patterns of Dune-Headland FST, CSS and Δp in *S. lautus*

(A) Relationship between the change in allele frequency (Δp) and F_{ST} comparing all Dune vs all Headland individuals, each datapoint representing a SNP. Red denotes the top 1% F_{ST} values. **(B)** Relationship of Δp to the cluster separation score (CSS). Red denotes the top 1% CSS values. **(C)** Relationship of F_{ST} and CSS. Red denotes the SNPs considered as outliers, being detected as outliers in at least two of the following approaches: top 1% F_{ST}, top 1% CSS, and *BayeScan* posterior probability > 0.91.

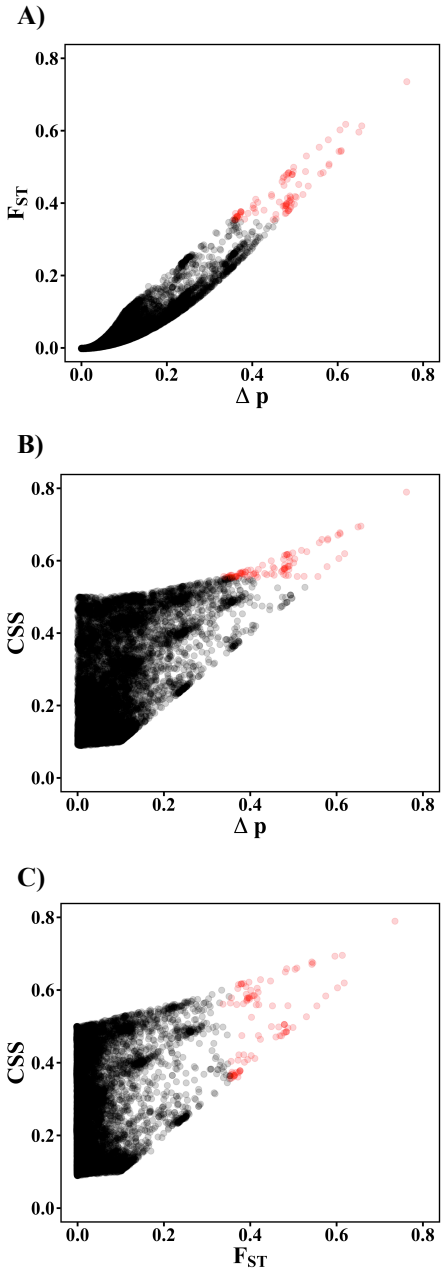

Figure S2. Principal components analysis of plant architecture and leaf traits in coastal ecotypes of *S. lautus*

Principal component analysis of Dune (orange) and Headland (green) phenotypes for **(A)** five plant architecture, and **(B)** four leaf traits across 20 populations. Ecotypes are delimited by 70% probability ellipses.

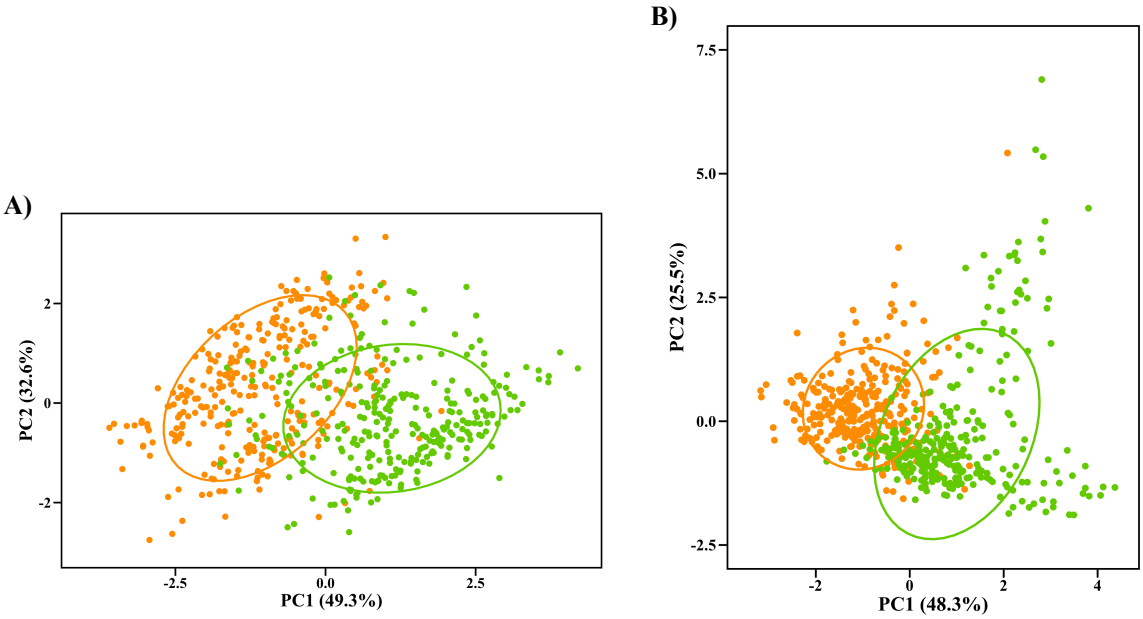

Figure S3. Trait-by-trait effect sizes in coastal ecotypes of *S. lautus*

Partial effect sizes (partial η^2) for the ecotype and pair for the trait-by-trait linear models, each dot representing a single trait. The red represents the partial effect size for all traits combined within the MANOVA. Dashed line is a 1:1 ratio, where points above the line represent a larger contribution of broad- to narrow-sense divergence. See Table S4 for details.

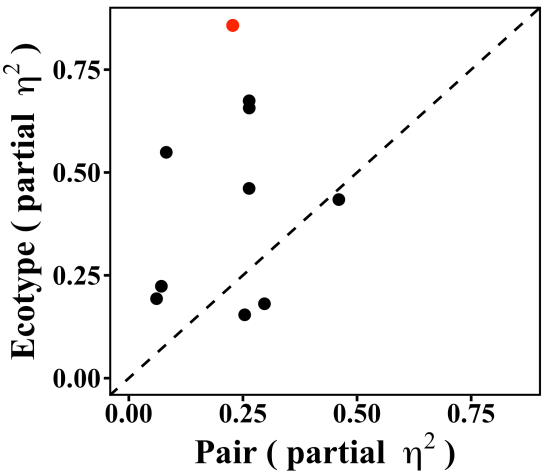

Figure S4. Phenotypic Change Vector Analysis for plant architecture traits in costal ecotypes from *S. lautus*

(A) PC1 and PC2 for five plant architecture traits across eight replicate Dune-Headland pairs. Each dot represents the population centroid (multivariate phenotypic mean), ± SE. The Dune (orange) and Headland (green) populations of a replicate pair are connected with a line. **(B)** Frequency distribution of the 28 pairwise phenotypic divergences (ΔL) between Dune-Headland replicate pairs (Supplementary Table S7). **(C)** Frequency distribution of the 28 pairwise contribution of traits (θ) between Dune-Headland replicate pairs (Supplementary Table S10).

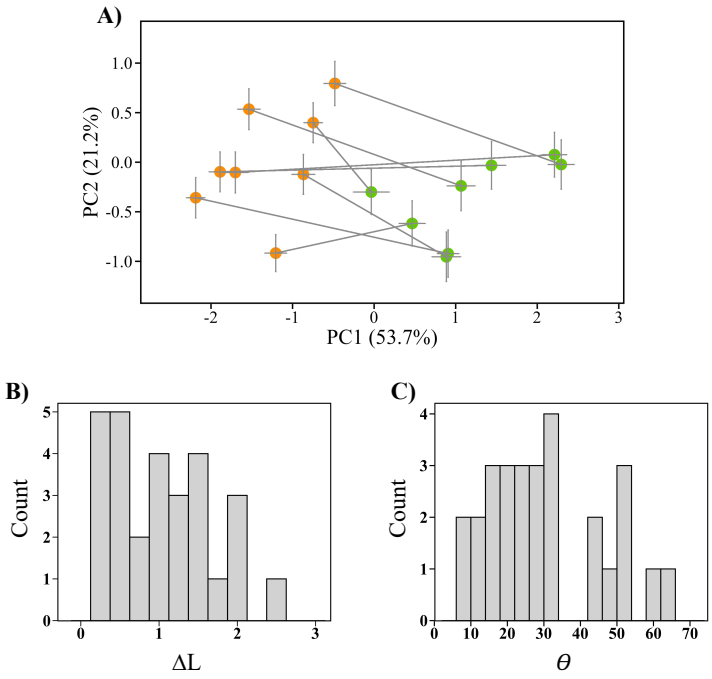

Figure S5. Phenotypic Change Vector Analysis for leaf traits in costal ecotypes from *S. lautus*

(A) PC1 and PC2 for four leaf traits across eight replicate Dune-Headland pairs. Each dot represents the population centroid (multivariate phenotypic mean), ± SE. The Dune (orange) and Headland (green) populations of a replicate pair are connected with a line. **(B)** Frequency distribution of the 28 pairwise phenotypic divergences (ΔL) between Dune-Headland replicate pairs (Supplementary Table S8). **(C)** Frequency distribution of the 28 pairwise contribution of traits (θ) between Dune-Headland replicate pairs (Supplementary Table S11).

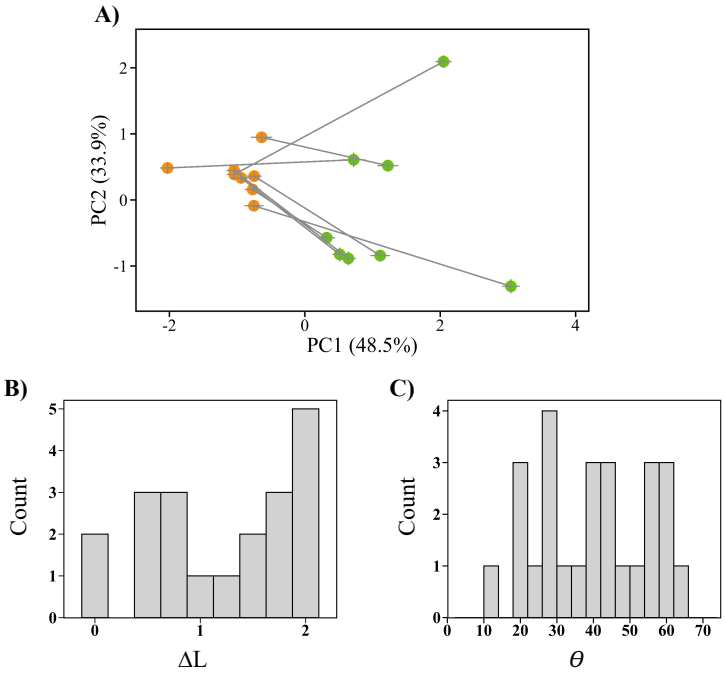

Figure S6. Relative contributions of broad- and narrow-sense genotypic parallelism

Partial effect sizes (partial η^2) for the ecotype and the pair for the linear models for nucleotide sites **(A)** genes **(B)**. Each dot represents either a single SNP **(A)** or gene **(B)**. Dashed line is a 1:1 ratio, where points above the line represent a larger contribution of broad- to narrow-sense parallelism. The red dotes denotes broad-sense outlier SNPs **(A)** and genes **(B)**. Partial effect size frequency distributions for the nucleotide sites **(C)** and genes **(D)**. Values above zero represent a larger contribution of broad- to narrow-sense parallelism.

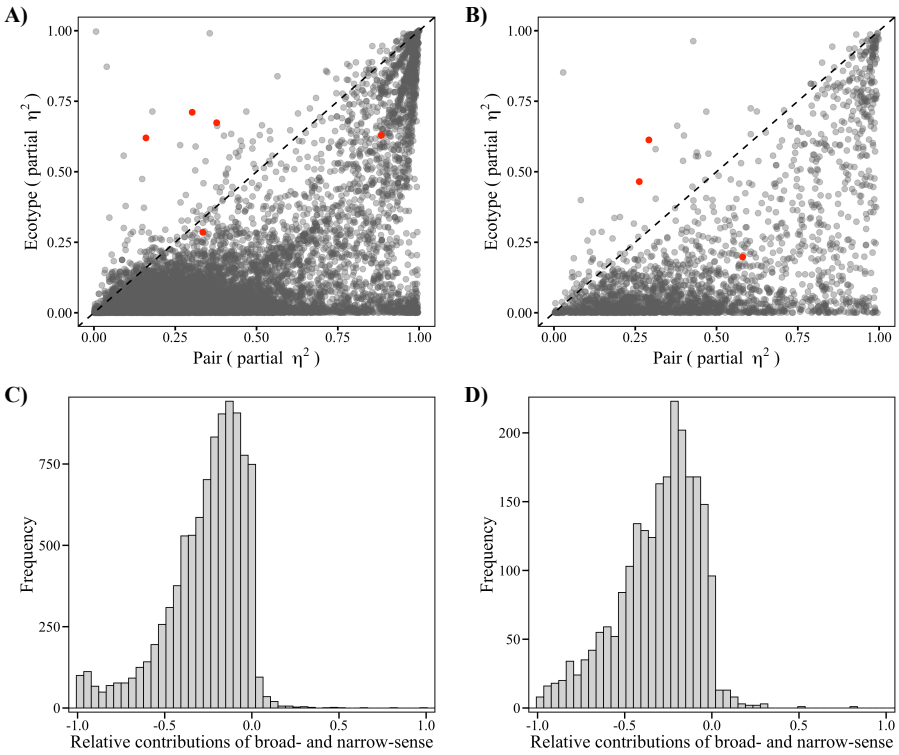

Figure S7. Broad-sense parallel nucleotide sites with concordant allele frequency differences

Broad-sense parallel nucleotide sites with concordant allele frequency differences (approach 2) in either all nine (S-statistic = 9, P = 0.004), or eight (S-statistic = 8, P = 0.04) replicate pairs. Dots represent the allele frequency value (of the reference allele) for each population. Lines connect the Dune (orange) populations to their Headland (green) pair. Dashed lines represent pairs whose Dune-Headland change in allele frequency is in the opposite direction from the majority of pairs. *G* denotes SNPs that occur within genic regions. These genes are as follows (left to right, top to bottom): *AT5G14540*, NA, *AT5G04420*, *CNGC1*, *OVA9*, *AT5G65740*, *EMB3144*, *HCT*. Asterisks denote SNPs that were also detected as outliers within approach 1 (see *Methods* for details).

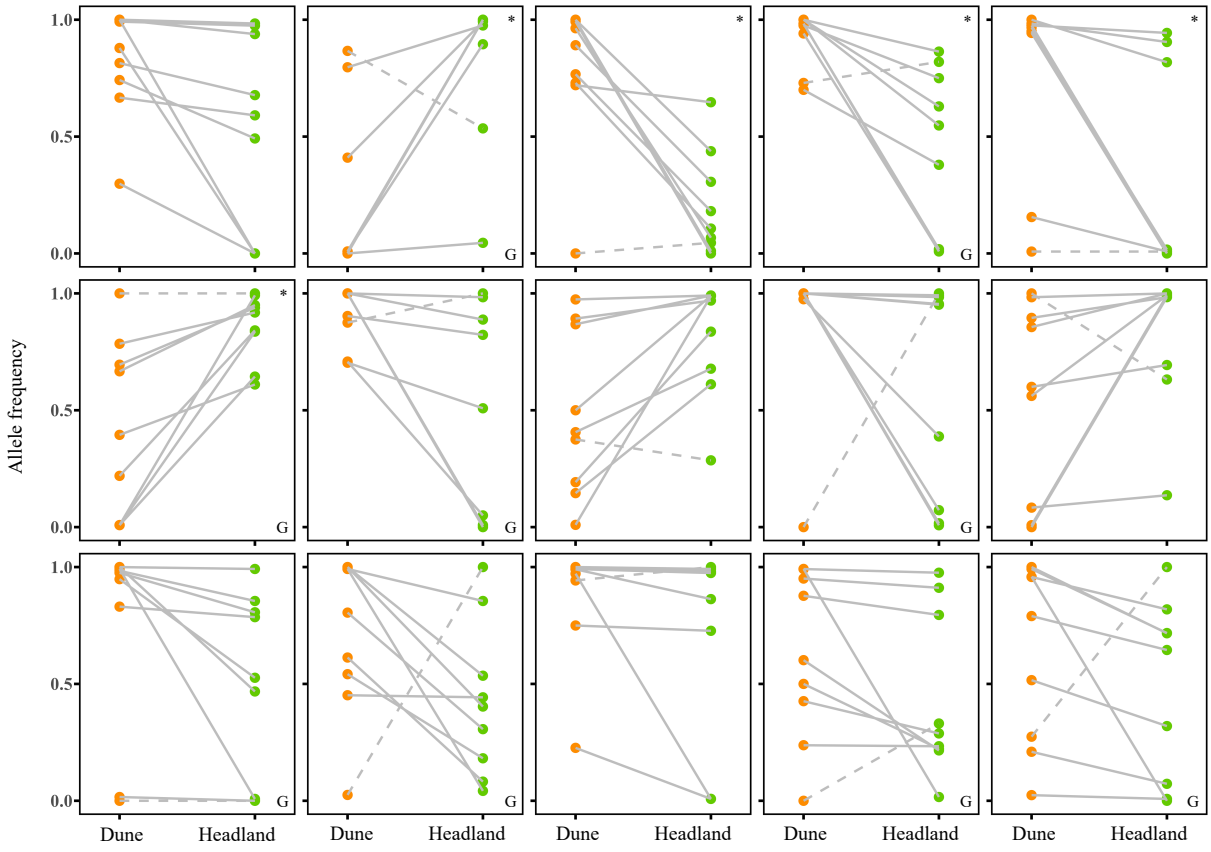

Figure S8. Broad-sense genotypic parallel evolution: nucleotide site and gene

Summary of the broad-sense outlier nucleotide sites and genes across approach 1 (blue box), approach 2 (green box) and the best candidates (orange box). See main text for details of each approach.

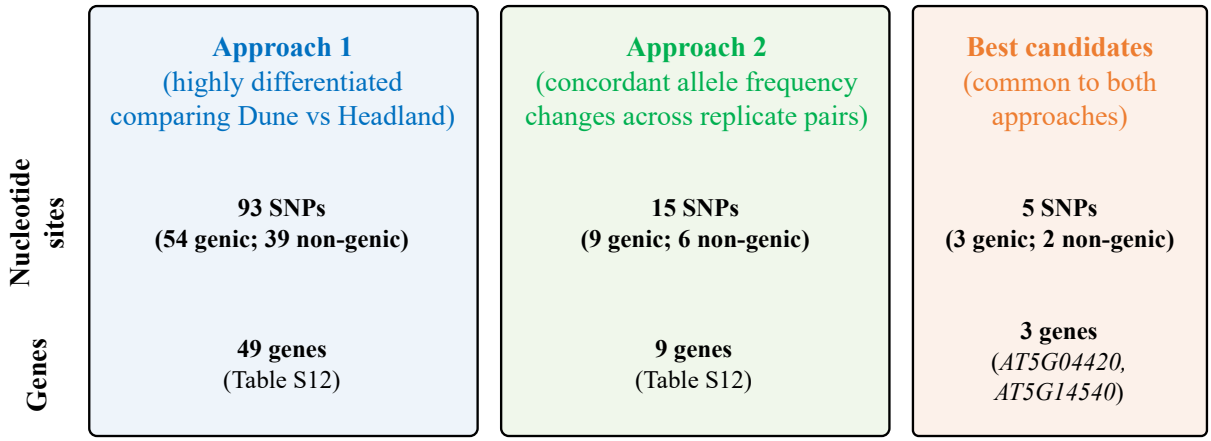

Supplementary R code

R code for Phenotypic Change Vector Analysis

```
# The following function estimates vector lengths, contrast, angles, and
# associated p values for differences between traits in multivariate space
# between two pairs of populations. Code adapted from Collyer & Adams (2007)

CollyerAdamsPCVA <- function(y.mat, x.mat, nPermutations = 9999) {
# First step: finalise the two x matrices (full and reduced)
x.mat.full<-x.mat
x.mat.red<-x.mat.full[,-4] # This removes the coding for the interaction effect

# Second step, estimate parameters for full and reduced models
b.mat.full<-solve(  (t(x.mat.full)%*%x.mat.full)  ) %*% (t(x.mat.full)%*%y.mat)
b.mat.red<-solve((t(x.mat.red)%*%x.mat.red))%*%(t(x.mat.red)%*%y.mat)

# Third step, Estimate LS means

# In this case, but not necessarily always, a = species and b = locality
# Vectors will be calculated for 2 species, a1 (P. jordani) and a2 (P. teyahalee)
# In our example the following dummy variables were used:
# P. jordani = 1, P. teyahalee = -1, sympatry = 1, allopatry = -1
# Thus, LS means could be calculated as follows:

a1b1<-cbind(1,1,1,1)
a1b2<-cbind(1,1,-1,-1)
a2b1<-cbind(1,-1,1,-1)
a2b2<-cbind(1,-1,-1,1)

x.ls.full<-rbind(a1b1,a1b2,a2b1,a2b2)
x.ls.red<-x.ls.full[,-4]

obs.ls.full<-x.ls.full%*%b.mat.full  # Observed ls means (full model)
obs.ls.red<-x.ls.red%*%b.mat.red     # Observed ls means (reduced model)

# Fourth Step, vector and statistics calculations

obs.a1.vect<-obs.ls.full[1,]-obs.ls.full[2,] # These are the phenotypic change vectors
obs.a2.vect<-obs.ls.full[3,]-obs.ls.full[4,]

obs.d.a1<-c(sqrt(t(obs.a1.vect)%*%obs.a1.vect)) # These are lengths of vectors
obs.d.a2<-c(sqrt(t(obs.a2.vect)%*%obs.a2.vect))

obs.contrast<-abs(obs.d.a1-obs.d.a2)
obs.angle<-c(acos(t((obs.a1.vect)/obs.d.a1)%*%((obs.a2.vect)/obs.d.a2)))
obs.angle<-obs.angle*180/pi  # This step is only necessary to convert radians to degrees

# Fifth Step, set-up permutation procedure

y.hat<-x.mat.red%*%b.mat.red     # Predicted values from reduced model
y.res<-y.mat-y.hat               # Resdiuals of reduced mode (these are the permuted units)

# PERMUTATION PROCEDURE

# Need to set-up distributions to be generated

dist.d1<-NULL
dist.d1<-rbind(dist.d1,obs.d.a1) # Observed value is first random value
dist.d2<-NULL
dist.d2<-rbind(dist.d2,obs.d.a2) # Observed value is first random value
dist.contrast<-NULL
dist.contrast<-rbind(dist.contrast,obs.contrast) # Observed value is first random value
dist.angle<-NULL
dist.angle<-rbind(dist.angle,obs.angle) # Observed value is first random value

# In addition to saving random values, it is wise to save the outcome of comparisons
# of observed and random values.
# This can be done with logical statements (below).
# Separate distributions are created for these comparisons.
# The 'p' indicates that these distributions will be used
# to calculate empirical probabilities.

pdist.contrast<-NULL
```

```
pdist.contrast<-rbind(pdist.contrast,1)
pdist.angle<-NULL
pdist.angle<-rbind(pdist.angle,1)

for(i in 1:nPermutations){
        y.res.rand <- y.res[sample(1:nrow(y.res)), ]

        # Create random values
        y.rand<-y.hat+y.res.rand

        # Estimate parameters
        b.mat.rand<-solve((t(x.mat.full)%*%x.mat.full))%*%(t(x.mat.full)%*%y.rand)

        # Calculate LS means
        rand.ls.full<-x.ls.full%*%b.mat.rand

        # Repeat fourth step for random data!

        rand.a1.vect<-rand.ls.full[1,]-rand.ls.full[2,] # These are the phenotypic change vectors
        rand.a2.vect<-rand.ls.full[3,]-rand.ls.full[4,]

        rand.d.a1<-c(sqrt(t(rand.a1.vect)%*%rand.a1.vect)) # These are lengths of vectors
        rand.d.a2<-c(sqrt(t(rand.a2.vect)%*%rand.a2.vect))

        rand.contrast<-abs(rand.d.a1-rand.d.a2)
        rand.angle<-c(acos(t((rand.a1.vect)/rand.d.a1)%*%((rand.a2.vect)/rand.d.a2)))
        rand.angle<-rand.angle*180/pi  # This step is only necessary to convert radians to degrees

        # Append distributions

        dist.d1<-rbind(dist.d1,rand.d.a1)
        dist.d2<-rbind(dist.d2,rand.d.a2)
        dist.contrast<-rbind(dist.contrast,rand.contrast)
        dist.angle<-rbind(dist.angle,rand.angle)

        aa<-ifelse(rand.contrast>=obs.contrast,1,0)
        bb<-ifelse(rand.angle>=obs.angle,1,0)

        pdist.contrast<-rbind(pdist.contrast,aa)
        pdist.angle<-rbind(pdist.angle,bb)
}

# Empirical probabilities are calculated as follows

 p.contrast<-sum(pdist.contrast)/(nPermutations+1)
 p.angle<-sum(pdist.angle)/(nPermutations+1)

 return(c(length.v1 = obs.d.a1,
        length.v2 = obs.d.a2,
        contrast = obs.contrast,
        p.contrast = p.contrast,
        angle = obs.angle,
        p.angle = p.angle))
}


# The following R code generates the required files to be used with the CollyerAdamsPCVA function

# 'master.file' is the entire phenotyping file, first column the pair, second column the ecotype,third column the population ID, the other columns the
phenotype data
master.file <- read.delim ("path-to-file/allTraitsPairs", header = TRUE)

# extract the unique elements of the first column (the pair)
pairs <- unique(master.file$Pair)

# create all possible pairwise comparisons
pairwise <-combn(pairs, 2)

# create empty data frame for the results
results <- data.frame(pair1 = pairwise[1,],
                pair2 = pairwise[2,],
                length.v1 = NA,
                length.v2 = NA,
                contrast = NA,
                p.contrast = NA,
                angle = NA,
                p.angle = NA)

for(i in 1:ncol(pairwise)) {
```

```
        # subset master file to generate proto-y.mat
        y.mat <- master.file[ master.file$Pair %in% pairwise[, i], ]

        # generate x.mat
        x.mat <- matrix(NA, nrow = nrow(y.mat), ncol = 4)  # empty matrix
        x.mat[,1] <- 1  # intercept
        x.mat[,3] <- 2 * (y.mat$Ecotype == "Dune") - 1  # 1 for dunes, -1 for headlands
        x.mat[,2] <- 2 * (y.mat$Pair == pairwise[1,i]) - 1  # 1 for pair 1, -1 for pair 2
        x.mat[,4] <- x.mat[,2] * x.mat[,3]  # interaction

        # modify y.mat to fit requirements
        y.mat <- as.matrix(y.mat[, -(1:3)])

        # run CollyerAdamsPCVA function on the two matrices
        results[i, 3:ncol(results)] <- CollyerAdamsPCVA(y.mat, x.mat)
}

write.table(results,file="path-to-file/PCVA_results.txt",row.names=FALSE,col.names=TRUE,quote=FALSE)
```

R code for cluster separation score (CSS)

```
#Define the path
path <- "/Users/maddiejames/Desktop/ESC/MDS/"
#Get a list of the input files (all files within the path)
allFiles <- list.files(path = path, pattern = "\\.mds$")
#Create a dataframe to store the data
CSSsnp <- data.frame(allFiles)
names <- c("CSS")
CSSsnp[ , names] <- NA
#Open each file and calculate CSS
for(k in 1:length(allFiles)) {
  MDSall<-read.delim(paste0(path,allFiles[k]), header=T, sep="")
  #Create the ecotype column
  ecotype<-substr(MDSall$IID, start = 1, stop = 1)
  MDSall<-cbind(Ecotype = ecotype, MDSall)
  #Replace the D with Dune and H with Headland
  MDSall$Ecotype <- gsub('D', 'Dune', MDSall$Ecotype)
  MDSall$Ecotype <- gsub('H', 'Headland', MDSall$Ecotype)
  #Subet the data into Dunes and Headlands
  MDSdune <- MDSall[MDSall$Ecotype=='Dune', ]
  MDSheadland <- MDSall[MDSall$Ecotype=='Headland', ]

  #Calculate the number of Dune individuals
  m <- nrow(MDSdune)
  #Calculate the number of Headland individuals
  n <-  nrow(MDSheadland)

  #Calculate the between group distance
  sumBetween <- 0
  for(i in 1:m) {
    for(j in 1:n) {
      sumBetween <- sumBetween + abs(MDSdune$C1[i] - MDSheadland$C1[j])
    }
  }

  #Calculate the within Dune distance
  sumWithinDune <- 0
  for(i in 1:(m-1)) {
    sumWithinDune <- sumWithinDune + abs(MDSdune$C1[i] - MDSdune$C1[i+1])
  }

  #Calculate the within Headland distance
  sumWithinHeadland <- 0
  for(j in 1:(n-1)) {
    sumWithinHeadland <- sumWithinHeadland + abs(MDSheadland$C1[j] - MDSheadland$C1[j+1])
  }

  #Calculate the CSS
  CSSsnp$CSS[k] <- sumBetween/(m*n) - (m+n)*(sumWithinDune/(m^2 * (m-1)) + sumWithinHeadland/(n^2 * (n-1)))
}

  #Print the results
write.table(CSSsnp, file="/Users/maddiejames/Desktop/ESC/CSSsnp_ESC.txt", row.names = FALSE, col.names = TRUE, quote = FALSE)
```